ANL-21/27

Identifying Limitations of ASME Section III Division 5 For Advanced SMR Designs

Applied Materials Division

About Argonne National Laboratory

Argonne is a U.S. Department of Energy laboratory managed by UChicago Argonne, LLC under contract DE-AC02-06CH11357. The Laboratory's main facility is outside Chicago, at 9700 South Cass Avenue, Argonne, Illinois 60439. For information about Argonne and its pioneering science and technology programs, see www.anl.gov.

ANL-21/27

Identifying Limitations of ASME Section III Division 5 For Advanced SMR Designs

Applied Materials Division
Argonne National Laboratory

June 2021

Prepared by

Mark C. Messner, Argonne National Laboratory

Ting-Leung Sham, Argonne National Laboratory[1]

Bipul Barua, Argonne National Laboratory

[1] Presently at Idaho National Laboratory

ABSTRACT

This report provides an overview of the ASME Boiler & Pressure Vessel Section III, Division 5 rules for the design and construction of high temperature nuclear reactor components. The overview focuses on the application of the rules to the design of Small Modular Reactors (SMRs). The discussion covers the general ASME Code rules for base metal design and construction, the rules for designing weldments, and provides an overview of environmental degradation mechanisms affecting reactor structural materials. The analysis includes historical context on the development of the ASME design approach and a description of what actions could be taken to mitigate the gaps identified in the report. The report concludes with a summary of the key gaps identified in the rules, as they apply to SMR, and a list of recommendations on how those gaps might be addressed.

TABLE OF CONTENTS

Abstract i
Table of Contents iii
List of Figures v
List of Tables vii
1 Introduction 1
1.1 Section III, Division 5 Scope 2
1.2 Summary 3
2 Division 5 Construction for Base Metal 5
2.1 Class B Construction 5
2.2 Class SM Construction 5
2.3 Non-nuclear Construction Rules 6
2.4 Division 5 Class A Construction 6
3 Design and Construction of Welded Components 31
3.1 Creep failure of weldments in high temperature service 31
3.2 ASME Section III, Division 5 rules 33
3.3 Time-temperature gaps 42
4 Design Under Advanced SMR Specific Environments 46
4.1 Failure mechanisms under irradiation 46
4.2 Failure mechanisms in corrosive environment 57
4.3 Gaps in ASME Section III, Division 5 rules and potential mitigation actions 60
5 Conclusions and Summary 63
5.1 Summary 63
5.2 Key recommendations 63
Acknowledgements 66
References 67

LIST OF FIGURES

Figure 2.1. The distribution of the stress component, σyy, through the wall thickness 8
Figure 2.2. Flow diagram for load-controlled primary load check 10
Figure 2.3. Flow diagram for strain limits, creep-fatigue and buckling checks 12
Figure 2.4. Illustration of the linearization procedure for the strain criteria in 1D 15
Figure 2.5. The distribution of the accumulated inelastic strain component, εyy, through the wall thickness 15
Figure 2.6. Bree diagram 16
Figure 2.7. Creep-fatigue interaction diagram 18
Figure 2.8. A typical fatigue design curve 21
Figure 2.9. Two general approaches to the stress relaxation profile: full-reset behavior, and one global relaxation history 23
Figure 2.10. Multiaxial relaxation calculated from uniaxial relaxation 24
Figure 3.1. Schematic of a weldment illustrating the Coarse-grained Heat Affected Zone (CHAZ), Fine-grained Heat Affected Zone (FHAZ) and the intercritical region, along with the weld and undisturbed base metal. The figure shows the location of a Type IV crack 31
Figure 3.2. Schematic of a cross-weld creep specimen. (a) shows how the specimen might be machined from a V-groove full penetration butt weld. The colors in the figure indicate the weld metal, CHAZ, FHAZ, intercritical zone, and base metal. (b) demonstrates the machined sample contains the entire weldment – weld, HAZ, and undisturbed base – in the sample gauge. 34
Figure 3.3. Schematic demonstrating the calculation of the weld stress rupture factor as the ratio of an extrapolated model for the weld average stress to rupture to the base metal average stress to rupture. 35
Figure 3.4. Demonstration of how for as-deposited welds the designer must include the stress concentration of the weld toe in their analysis. 39
Figure 3.5. Illustration of the basic categorization of welds in a vessel. Note that the weld connecting the hemispherical head to the shell is an example of an exception from the general classification scheme: it is a circumferential joint but is category A (not category B) because it connects a hemispherical head to the vessel shell. 40
Figure 4.1. A general overview of the temperature regimes where different radiation-induced degradation mechanisms are most prominent in structural alloys [33]. 47
Figure 4.2. Comparison of tensile strength between unirradiated and irradiated Alloy 617 (top) and Alloy 800H (bottom). Total irradiation was about 1.42 dpa and 1.45 dpa, respectively for Alloy 617 and Alloy 800H. Trend line from [36]. 48
Figure 4.3. The trend in yield strength of several solution annealed type 316 and PCA austenitic stainless steels as a function of temperature. The irradiation temperature is equal to the test temperature and the neutron doses range from 3 to 20 dpa. Trend line from [37]. 49
Figure 4.4. The trend in yield strength evolution as a function of temperature, neutron irradiation, and heat treatment for type 316 austenitic stainless steel. Trend line from [38]. 49
Figure 4.5. Comparison of total tensile elongation between unirradiated and irradiated Alloy 617 (top) and Alloy 800H (bottom). Total irradiation was about 1.42 dpa and 1.45 dpa, respectively for Alloy 617 and Alloy 800H. Trend line from [36]. 50
Figure 4.6. Temperature dependence of in-reactor and thermal creep for 20% cold worked Type 3 16 stainless steel. Trend line from [40]. 51
Figure 4.7. Swelling as a function of irradiation temperature and dose, as observed for 20% cold-worked type 316 austenitic steel irradiated in the EBR-II fast reactor. Trend line from [44]. 52

Figure 4.8. Comparison of swelling in type 304L and cold-worked 316 austenitic stainless steels and 9-12 Cr ferritic/martensitic steel, as irradiated at ~400-550°C to high doses in a fast fission spectrum. Trend line from [46]. 54
Figure 4.9. Effect of nickel content on swelling behavior of Fe-Cr-Ni alloys. Trend line from [49]. 55
Figure 4.10. Comparison between fatigue and creep-fatigue lives of Alloy 617 in air and impure helium environments at 950°C. The applied strain range was 0.6% and all the hold times were applied in tension. The in-air data were taken from [95] and the in-impure helium from [94]. 60

LIST OF TABLES

Table 1.1. ASME Section III, Division 5 Organization 2
Table 2.1. Construction rules selection for metallic components. 5
Table 2.2. Structural failure modes and design evaluation procedures for Class A components. 7
Table 2.3. General description of service loadings in HBB. 8
Table 2.4. Example of classification of stress intensity for a flat head vessel 9
Table 2.5. Linearized stresses for computing stress intensity for the primary load acceptance criteria 11
Table 2.6. Design analysis methods for assessing deformation controlled limits for Class A components 13
Table 2.7. Temperatures above which consideration of viscoplastic effect is required 13
Table 2.8. Characteristics of simplified methods for strain limits 17
Table 2.9. Intersections of the bilinear creep-fatigue damage envelope for Class A materials 19
Table 2.10. Values of C for equivalent stress 20
Table 2.11. Values of K' for inelastic analysis 20
Table 2.12. Values of K' for elastic analysis 25
Table 2.13. Time-dependent load-controlled buckling factors. 26
Table 2.14. Temperatures and time ranges of design parameters for base metals – List 1 29
Table 2.15. Temperatures and time ranges of design parameters for base metals – List 2 29
Table 2.16. Temperatures and time ranges of design parameters for bolt materials 29
Table 2.17. Max. temperature conditions on allowable stresses 30
Table 3.1. Summary of allowable base/weldment combinations with time/temperature gaps highlighted 43
Table 4.1. Summary of SMR designs based on core exit temperature [31]. 46
Table 4.2. Effect of sodium exposure on fatigue and creep-fatigue life of modified 9Cr-1Mo steel [45]. 58

1 Introduction

The construction rules for the structural components of high temperature reactors have had a long history of development. Elevated temperature design rules for nuclear components were initiated in 1963 with American Society of Mechanical Engineers (ASME) Code Case 1331. Complete construction rules for elevated temperature pressure boundary metallic components under cyclic service were first published in the early 1970s in a series of ASME Code Cases, 1592, 1593, 1594, 1595 and 1596 for materials and design, fabrication and installation, examination, testing, and overpressure protection, respectively. The U.S. Nuclear Regulatory Commission (USNRC) issued Regulatory Guide 1.87 (Rev 1, June 1975), referencing the ASME Code Case series 1592 to 1596, to provide interim licensing guidelines to aid applicants in implementing the U.S. 10 CFR Part 50 requirements in supporting the licensing of ASME Boiler and Pressure Vessel Code (BPVC) Class 1 components operating at elevated temperatures for high-temperature gas-cooled reactors, liquid-metal fast-breeder reactors, and gas-cooled fast-breeder reactors.

This Code Case series was converted to Code Case N-47 when the nuclear code cases were separated from the non-nuclear code cases by ASME. Code Case N-47 was used by the Clinch River Breeder Reactor (CRBR) project, with additional requirements from the U.S. Department of Energy (USDOE), for the structural design of CRBR. A license application for a construction permit for CRBR was submitted by USDOE to USNRC for approval in the late 1970s. Assessment of the construction rules of Code Case N-47 by USNRC was in progress when the CRBR project was cancelled by the U.S. Government.

Continued improvements of the rules of N-47 had been made since then, and the code case was subsumed into a new Section III, Division 1, Subsection NH in 1995 by ASME. Extension of the rules of construction of Division 1 Class CS core support structures and Division 1 Class 2 components to elevated temperature service was made in a series of nuclear code cases, N-201, N-253, N-254, N-257, and N-467.

The Energy Policy Act of 2005 passed by the U.S. Congress established the Next Generation Nuclear Plant (NGNP) Program to demonstrate the generation of electricity and/or hydrogen with a high-temperature nuclear energy source. The Idaho National Laboratory (INL) was the lead USDOE Laboratory responsible for the execution of the NGNP Program. In order to reduce regulatory risks for the licensing of the NGNP reactor plant with the USNRC, it was deemed desirable to streamline the applicable Codes and Standards. INL requested ASME to develop a new Division within Section III to consolidate all high temperature construction rules in Subsection NH and the other nuclear code cases and to add the construction rules for graphite core components to the new Division to support the NGNP. The new Section III, Division 5 was published in the 2011 Addenda of the ASME BPVC. Continued updates and improvements of the construction rules of Section III, Division 5 have taken place since its initial publication.

Consensus Codes and Standards have been integral to the USNRC's regulatory process for light water reactors. They promote safe operation of nuclear power plants and improve effectiveness and efficiency of regulatory oversight. ASME BPVC Section III, Division 5 is deemed essential by developers in supporting the deployment of advanced reactors. However, a lack of USNRC

endorsement of the ASME construction rules for high temperature reactors represents a significant regulatory risk for the commercial deployment of advanced nuclear.

This subject was brought to the forefront in 2015 and the adverse impacts of a lack of regulatory endorsement of ASME Section III, Division 5 were broadly recognized by USNRC, USDOE and the advanced reactor industry. With support from the advanced reactor developers, ASME made a request to USNRC in 2018 for the endorsement of Section III, Division 5 [1]. USNRC subsequently agreed to initiate efforts to review the 2017 Edition of ASME BPVC Section III, Division 5 [2]. The USNRC endorsement effort is currently ongoing.

1.1 Section III, Division 5 Scope

ASME Section III, Division 5 rules govern the construction of vessels, piping, pumps, valves, supports, core support structures and nonmetallic core components for use in high temperature reactor systems and their supporting systems. The term construction, as used in the context of ASME Section III, is an all-inclusive term that includes material, design, fabrication, installation, examination, testing, overpressure protection, inspection, stamping, and certification.

Division 5 contains six Subsections, covering Code Classes A, B and SM for metallic coolant boundary components and supports and Code Class SN for nonmetallic core components. The organization of Division 5 is shown in Table 1.1.

Table 1.1. ASME Section III, Division 5 Organization

Code Class	Sub-section	Subpart	Subsection ID	Title	Scope
General Requirements					
Class A, B, & SM	HA	A	HAA	Metallic Materials	Metallic
Class SN		B	HAB	Graphite and Composite Materials	Nonmetallic
Class A Metallic Coolant Boundary Components					
Class A	HB	A	HBA	Low Temperature Service	Metallic
Class A		B	HBB	Elevated Temperature Service	Metallic
Class B Metallic Coolant Boundary Components					
Class B	HC	A	HCA	Low Temperature Service	Metallic
Class B		B	HCB	Elevated Temperature Service	Metallic
Class A and Class B Metallic Supports					
Class A & B	HF	A	HFA	Low Temperature Service	Metallic
Class SM Metallic Core Support Structures					
Class SM	HG	A	HGA	Low Temperature Service	Metallic
Class SM		B	HGB	Elevated Temperature Service	Metallic
Class SN Nonmetallic Core Components					
Class SN	HH	A	HHA	Graphite Materials	Graphite
Class SN		B	HHB	Composite Materials	Composite

ASME Section III, Division 5 recognizes the different levels of importance associated with the function of each component as related to the safe operation of the reactor plant. The Division 5 Code Classes allow the choice of appropriate rules commensurate with the relative importance of the safety functions assigned to individual component. But Section III, Division 5 is a "Component Code" and does not contain rules for the safety classification of individual component. Component classification is performed at the system level.

The Division 5 requirements do not cover deterioration that may occur in service as a result of radiation effects, corrosion, erosion, thermal embrittlement, or instability of the material. Thus, these materials degradation effects are outside the scope of Section III, Division 5 and they shall be accounted for by the owner/operator.

1.2 Summary

This report contains both a summary of the ASME Section III, Division 5 design rules and a gap analysis focusing on SMR designs and expected operating conditions. Chapter 2 covers the rules for base metal and Chapter 3 the rules for the design and construction of weldments. Chapter 4 covers the design of components operating in expected future SMR environments. As discussed in that Chapter, the ASME rules do not explicitly cover environmental effects, leaving that instead for the owner to account for in order to satisfy any regulatory requirements. This chapter then describes the likely negative environmental effects future SMRs are likely to encounter and summarizes potential strategies to account for these effects, in part by referencing non-ASME standards. Finally, Chapter 5 summarizes the report, focusing on the SMR gap analysis.

2 Division 5 Construction for Base Metal

The approach to the selection of appropriate Code Classes for structural components of high temperature reactor systems starts with the safety classification per safety criteria from applicable standards and based on a system approach. In general, applicable construction rules for metallic components can be selected based on component safety classification as shown in Table 2.1.

Table 2.1. Construction rules selection for metallic components.

Metallic	Classification	Construction Rules
Coolant boundary components and supports	Safety related	Section III, Division 5, Class A
	Non-safety related with special treatment	Section III, Division 5, Class B
	Non-safety related	Appropriate non-nuclear codes and standards
Core support structures	Safety related	Section III, Division 5, Class SM

For each Division 5 metallic Code Class, construction rules for low temperature service are applicable when the component metal temperature is at or below 700°F (371°C) for ferritic materials and 800°F (427°C) for austenitic materials. This is the temperature regime where the creep effect, if any, does not reduce the cyclic performance of the material. Construction rules for elevated temperature service apply when the component metal temperature exceeds 700°F (371°C) for ferritic materials and 800°F (427°C) for austenitic materials.

2.1 Class B Construction

The Division 5 Class B rules are the extension of the construction rules of Division 1, Class 2 vessel, pump, valve and piping design rules to elevated temperature service. Class B rules are based on the design-by-rule approach. Fatigue damage resulting from cyclic service is not addressed for vessel, pump and valve. It is also not addressed for piping in the negligible creep regime. For piping with creep effects, rules are provided to address fatigue damage from cyclic service. Though the Class B piping rules which account for the effects of creep-fatigue damage are different from those for Class A piping. It is noted that unlike Class A and Class SM rules, the concept of design lifetime is not used in Class B rules.

As an alternative to the Class B rules, a component designated as Class B may use the Class A rules for construction, but all the applicable Class A requirements shall be used. If this option is selected, all the applicable Class B requirements shall not be used except that the component remains designated and stamped as a Class B component. This essentially allows a component that is classified as Class B for safety consideration but constructed using Class A rules to address structural integrity issues under cyclic service, possibly as a protection of investment.

2.2 Class SM Construction

The Division 5 Class SM rules are the extension of the construction rules of Division 1, Subsection NF for core support structures, internal structures, threaded structural fasteners, and temporary attachments to elevated temperature service. The load-controlled design rules are very similar to those for Class A rules. However, consistent with the low temperature rules, the Design Loading is not used and pressure difference, instead of pressure, is considered. For deformation-controlled

limits, the Class A rules in Appendix HBB-T are referenced directly. However, any applications that are appropriate for Class A components but not for Class SM supports are identified.

2.3 Non-nuclear Construction Rules

For non-safety related metallic components, non-nuclear codes and standards may be used and they include ASME BPVC Section VIII, Division 1 or Division 2 for vessel and ASME B31.3 for piping. Section VIII, Division 1 and Division 2 cover pressure vessel design for both low and elevated temperature service. The Section VIII, Division 1 rules are based on the design-by-rule approach and do not cover cyclic service. Section VIII, Division 2 rules are based on the design-by-analysis approach, but only cover cyclic service in the low temperature regime. The temperature boundary between low temperature and elevated temperature service is the same as Section III, Division 5. The duration of the design lifetime is not considered in the Section VIII rules.

2.4 Division 5 Class A Construction

The main focus of this report is on Class A elevated temperature construction rules in Division 5, Subsection HB, Subpart B (HBB).

2.4.1 Structural failure modes

The Division 5 Class A design rules are based on the design-by-analysis approach. The rules seek to provide a reasonable assurance of adequate protection of structural integrity and are based on design against structural failure modes. The structural failure modes that are addressed in the low temperature service regime are time independent and they include:

- Ductile rupture from pressure
- Gross distortion (ratcheting) due to cyclic mechanical and thermal loading
- Fatigue failure due to cyclic mechanical and thermal loading
- Buckling due to compressive load

For elevated temperature service, additional time and temperature dependent failure modes are involved and they are:

- Creep rupture due to sustained pressure load
- Creep ratcheting due to cyclic mechanical and thermal loading
- Creep-fatigue failure due to cyclic mechanical and thermal loading
- Creep buckling due to sustained compressive load

2.4.2 Design evaluation procedures

The failure modes for low temperature and elevated temperature service can be categorized into load-controlled or deformation-controlled failure modes. Protection against these failure modes can be achieved with reasonable assurance by four design evaluation procedures, each with a set of acceptance criteria. The four design evaluation procedures are:

- Load-controlled: Primary load check
- Deformation-controlled: Strain limits check, creep-fatigue check, buckling check

The failure modes and their corresponding design evaluation checks are shown in Table 2.2.

Table 2.2. Structural failure modes and design evaluation procedures for Class A components.

Time Independent Failure Mode	Category	Design Evaluation Procedure	Time Dependent Failure Mode	Category	Design Evaluation Procedure
Ductile rupture from short-term loading	Load-controlled	Primary load check	Creep rupture from long-term loading	Load-controlled	Primary load check
Gross distortion due to incremental collapse and ratcheting (low temperatures)	Deformation-controlled	Strain limits check	Creep ratcheting due to cyclic service	Deformation-controlled	Strain limits check
Loss of function due to excessive deformation	Deformation-controlled	Strain limits check	Creep-fatigue failure due to cyclic service	Deformation-controlled	Creep-fatigue check
Buckling due to short-term loading	Deformation-controlled	Buckling Check	Creep-buckling due to long-term loading	Deformation-controlled	Buckling Check

The operating pressure of advanced reactor systems ranges from atmospheric, such as sodium fast reactor or molten salt reactor, to a modest magnitude such as gas-cooled high temperature reactor where the pressure is close to that in a boiling light water reactor. However, even for a low pressure advanced reactor system under cyclic service, structural integrity of its components would still need to be addressed as failure modes such as creep ratcheting and creep-fatigue damage caused by thermal transients in the reactor plant are present.

Loading categories. The four design evaluation checks that provide protection against the structural failure modes identified in the previous section for Class A components are performed by the Designer based on the loading information provided in the Design Specification by the Owner, as stipulated in the requirements of BPVC Section III, Subsection NCA. The loading information consists of the expected history of pressures, temperatures and mechanical load forces as a function of time, and a list of events that occur under each loading category.

While it is challenging to prescribe with some certainty the exact sequence of events for 30 to 60 years of operation, the Owner and Regulator agree on a specified sequence of events that will provide a reasonable expectation of safe operation.

The loading categories supporting the design evaluation checks in HBB include Design Loading, Service Loadings, and Test Loadings. The Design Loading category shall equal or exceed those of the most severe combination of coincident pressure, temperature, and load forces specified under events which cause Service Level A Loadings. The Service Loadings consist of Levels A, B, C, and D as shown in Table 2.3.

Table 2.3. General description of service loadings in HBB.

Service Level	Description
A	Planned operations
B	Expected but unplanned events that does not require shutdown for inspection or repair
C	Unusual possible events that require shutdown for inspection and potential repair
D	Postulated events that the integrity and functionality of the nuclear energy system may be impaired to the extent that only considerations of public health and safety are involved

Test Loadings are pressure loadings that occur during hydrostatic tests, pneumatic tests, and leak tests.

2.4.3 Load-controlled design evaluations

2.4.3.1 Primary load check.

The primary load check in HBB is based on the elastic analysis of a reactor structure subject to self-equilibrating external loads. The resulting stresses satisfy the equilibrium equations within the structure and give rise to tractions on the external surface of the structure that satisfy the traction boundary condition. The use of inelastic analysis to conduct the primary load check is currently not permitted in HBB.

Stress linearization. The stresses across a particular cross-section through the wall thickness of the structure, e.g., the σ_{yy} stress component shown in Figure 2.1, are subject to a stress linearization procedure to determine the so-called primary membrane stresses, $\sigma_{ij,m}$, and primary bending stresses, $\sigma_{ij,b}$:

$$\sigma_{ij,m} = \frac{1}{t}\int_0^t \sigma_{ij}(x)dx \quad i,j = 1,2,3$$

$$\sigma_{ij,b} = \frac{6}{t^2}\int_0^t \sigma_{ij}(x) \times \left(\frac{t}{2} - x\right) dx \quad i,j = 1,2,3$$

where σ_{ij} are the stress components, and t is the wall thickness.

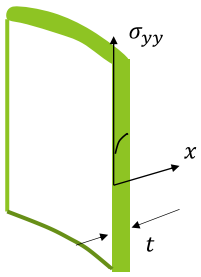

Figure 2.1. The distribution of the stress component, σ_{yy}, through the wall thickness.

Stress intensity. The three-dimensional stresses obtained from the stress linearization procedure are used to determine a scalar stress measure called the stress intensity which is defined as twice the maximum shear stress calculated from the three-dimensional linearized stresses. The stress

intensity can be computed as the absolute value of the difference between the maximum and minimum principal stresses.

Stress classification. The stress intensities determined from the primary membrane stresses and the primary bending stresses are assigned to different categories. This process is called stress classification and it is dependent on the geometry of the structure, the location of the cross-section where the linearization procedure is performed, the type of applied load, and the type of stress. Engineering judgment is often required. Some of the categories are as follows:

- P_m = Primary membrane stress components
- P_L = Local primary membrane stress components
- P_b = Primary bending stress components at a surface
- Q = Secondary stress components

An example of the stress classification of a flat head vessel from HBB is shown in Table 2.4.

Table 2.4. Example of classification of stress intensity for a flat head vessel

Vessel Component	Location	Origin of Stress	Type of Stress	Classification
Flat head	Center region	Internal pressure	Membrane	P_m
			Bending	P_b
	Junction to shell	Internal pressure	Local Membrane	P_L
			Bending	Q

Limits for load-controlled stresses. Allowable stresses are defined in terms of tensile strengths and creep rupture strength for use as limits to guard against the load-controlled failure modes. They are defined for base metal as follows:

S_m = lesser of:

a) one-third of the specified minimum tensile strength at room temperature

b) one-third of the tensile strength at temperature

c) two-thirds of the specified minimum yield strength at room temperature

d) two-thirds of the yield strength at temperature

S_t = lesser of:

a) 100% of the average stress required to obtain a total (elastic, plastic, primary, and secondary creep) strain of 1%;

b) 80% of the minimum stress to cause the onset of tertiary creep; and

c) 67% of the minimum stress to cause rupture

S_{mt} = lesser of (S_m, S_t)

S_0 = lesser of $(S, S_{mt}@300{,}000h)$

where S is the tabulated allowable stress in Section II, Part D Table 1A (ferrous materials) or Table 1B (nonferrous materials

Acceptance criteria. Since the stress intensities determined from elastic stress analysis results are used in the primary load check to address inelastic structural failure modes, a rather complicated set of acceptance criteria were required to provide a reasonable assurance to guard against these load-controlled failure modes. The acceptance criteria are given in Figure 2.2. The parameters K and K_t are shape factors that depend on the cross-sectional geometry of the cross-section of wall.

For the time fraction t_i/t_{im} in Figure 2.2, t_i is the total duration at P_{im}; t_{im} is the maximum allowed time for P_{im}, as determined from S_t-vs-time plot; $B \ll 1$, with the exact value given in the Design Specification. For the time fraction t_i/t_{ib} in Figure 2.2, t_i is the total duration at $P_L + P_b/K_t$, t_{ib} is the maximum allowed time for $P_L + P_b/K_t$, as determined from S_t-vs-time plot.

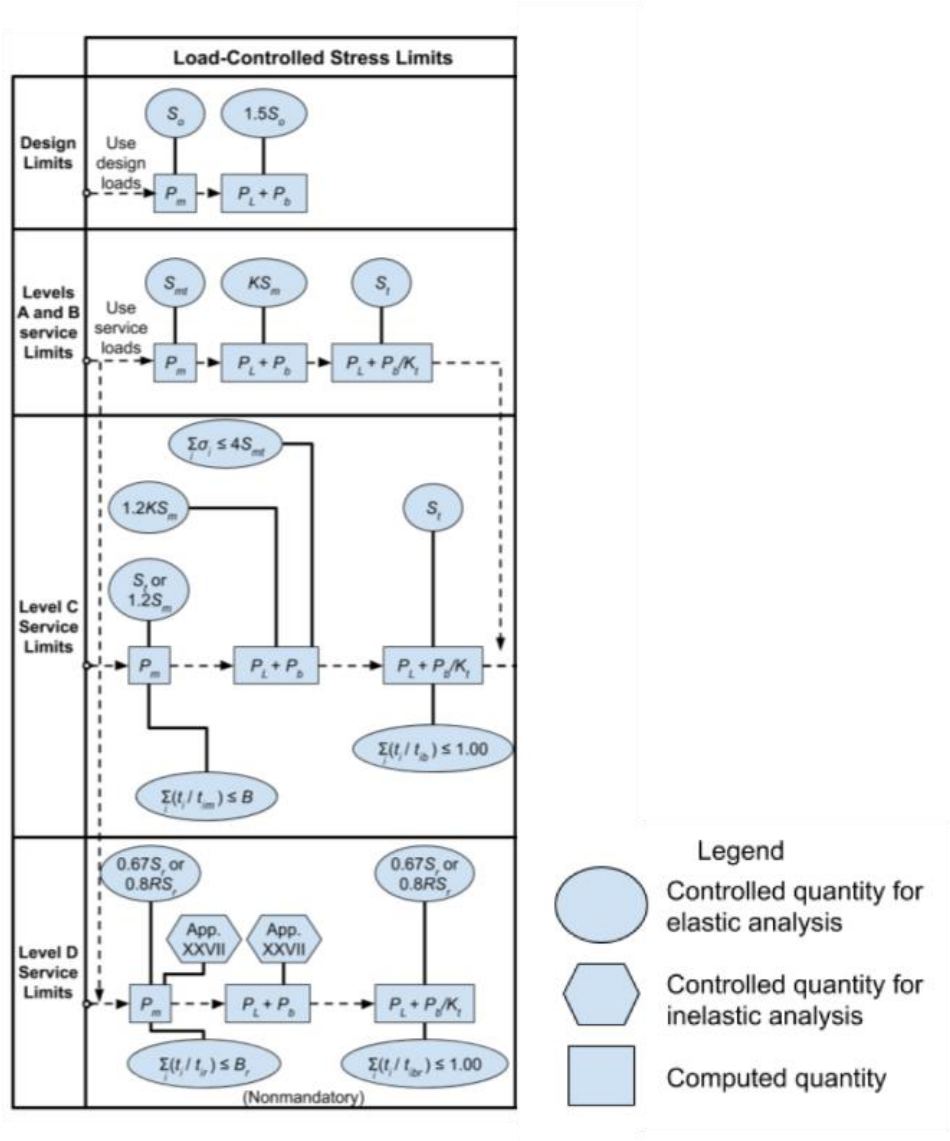

Figure 2.2. Flow diagram for load-controlled primary load check

The determination of the appropriate stress intensity from the linearized stress components for each of the acceptance criteria in Figure 2.2 is shown in Table 2.5.

Table 2.5. Linearized stresses for computing stress intensity for the primary load acceptance criteria

Stress intensity	Linearized stresses used to compute stress intensity
$\boldsymbol{P_m}$	$\sigma_{ij,m}$
$\boldsymbol{P_L + P_b}$	$\sigma_{ij,m} + \sigma_{ij,b}$
$\boldsymbol{P_L + P_b/K_t}$	$\sigma_{ij,m} + \sigma_{ij,b}/K_t$

2.4.4 Deformation-controlled design evaluations

The acceptance criteria for the deformation-controlled limits in HBB are shown in the flow diagram of Figure 2.3.

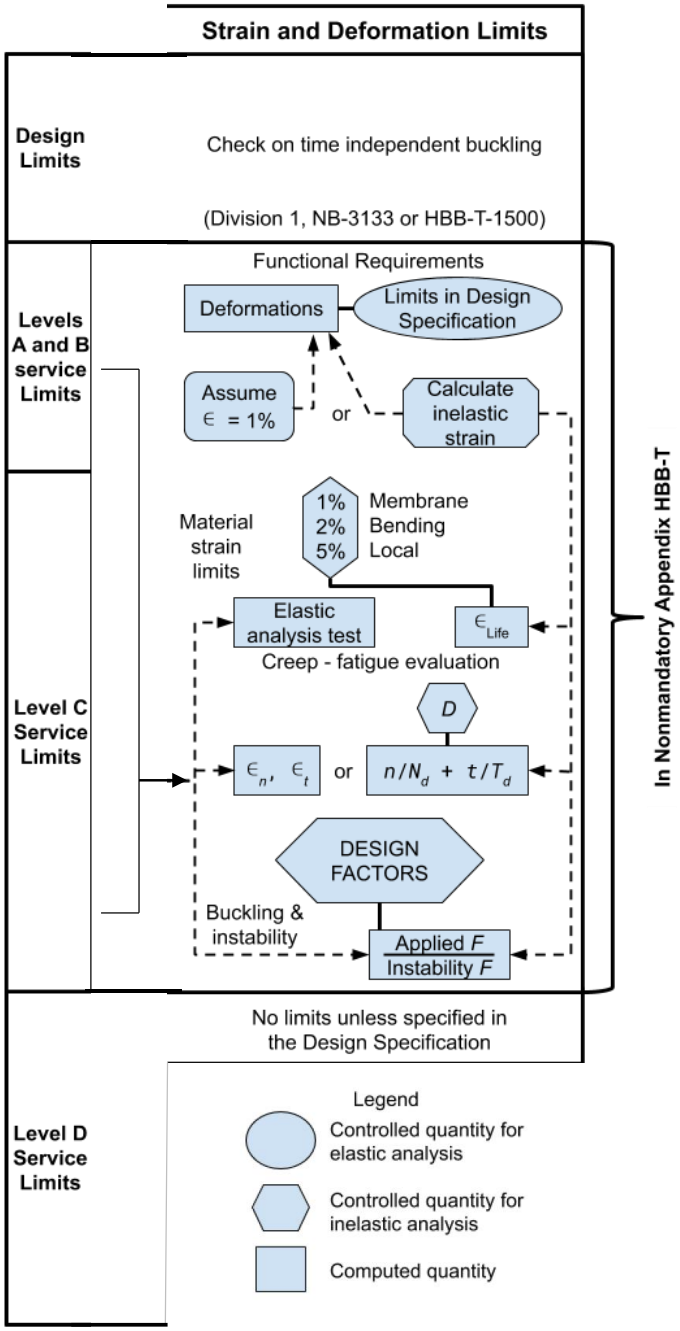

Figure 2.3. Flow diagram for strain limits, creep-fatigue and buckling checks

Two analysis approaches, use of elastic analysis or inelastic analysis results, are permitted in HBB to conduct the strain limits, creep-fatigue and buckling checks as summarized in Table 2.6. The steps to assess the satisfaction of the acceptance criteria/design limits for these two approaches are different.

Table 2.6. Design analysis methods for assessing deformation-controlled limits for Class A components

Deformation controlled limits	Use of elastic analysis result	Use of inelastic analysis result
Strain limits check	Permitted	Permitted
Creep-fatigue check	Permitted	Permitted
Buckling check	Use Section II pressure charts referenced by Division 1, NB-3133 when temperature limits are satisfied for specific geometries and loading	Permitted

Use elastic analysis results. Inelastic analysis is generally required to provide a quantitative assessment of deformations and strains when creep effects are present. However, design evaluation methods based on the use of elastic analysis results may sometimes be justified to provide conservative bounds for deformations, strains, strain ranges, and maximum stress to guard against the identified structural failure modes.

These methods are intended as "screening" tools. They rely on linearization and stress classification to extract results from the elastic stresses and some bounding criteria to address inelastic failure modes. The establishment of the bounding criteria was based on materials deformation models where creep and plasticity do not interact. This fundamental assumption would start to break down at higher temperatures and reduce the design margins. A recent ASME Code committee effort to quantity the temperatures where this transition takes place is documented in Messner et al. [3] and ASME C&S Record 15-2735. The temperatures above which consideration of viscoplastic effect is important are shown in Table 2.7.

Table 2.7. Temperatures above which consideration of viscoplastic effect is required

Class A material	Temperature limit (°C)	Temperature limit (°F)
Type 304 stainless steel	625	1150
Type 316 stainless steel	650	1200
Alloy 800H	710	1310
2¼Cr-1Mo	550	1020
9Cr-1Mo-V	450	840
Alloy 617	635	1175

Use inelastic analysis results. The design evaluation methods based on the use of inelastic analysis results to perform deformation-controlled checks (strain limits, creep-fatigue and buckling) are more accurate and less conservative as compared with the methods based on elastic stresses. They are intended for use to check the "hot spots" where the designs do not meet design limits based on the conservative elastic methods. This was the case for the CRBR steam generator design where inelastic finite element results had to be used in order to meet the design limits. The inelastic material models were developed by the USDOE national laboratory and provided to the CRBR contractors for the design analyses. Currently, Division 5 (2019 Edition) does not specify the

inelastic constitutive models that are appropriate for use in the inelastic design evaluation methods. The responsibility of specifying the inelastic constitutive models appropriate to support Class A designs resides with the Owner or the Designer. But the models would have to be justified to Jurisdictional Regulator. This limits the application of the inelastic analysis approach for design evaluations.

There is an ongoing long-term technical effort by the ASME Code committee to establish guidelines for inelastic material models development, and to develop inelastic constitutive equations for the Class A materials. The guidelines have been implemented in a new Appendix HBB-Z that is currently being balloted by ASME. Included in the same action are the viscoplastic constitutive equations for Grade 91 steel, with the material parameters specified as functions of temperatures to support applications, Messner et al [4]. The ASME C&S Record for this action is RC 19-317. The next viscoplastic constitutive equations to be added to Appendix HBB-Z will be Alloy 617, followed by Type 316 stainless steel, Phan et al [5] and then Alloy 800H.

2.4.4.1 Strain limits check

The strain limits are given in Division 5 paragraph HBB-T-1310 and they require that the maximum accumulated inelastic strain over any cross-section of the wall thickness of the structure shall not exceed the following:

a) strains averaged through the thickness, 1%

b) strains at the surface, due to an equivalent linear distribution of strain through the thickness, 2%

c) local strains at any point, 5%.

The above limits apply to computed inelastic strains accumulated over the expected operating lifetime of the element under consideration, and computed for some steady-state period at the end of this time during which significant transients are not occurring.

These strain limits were established based on Codes and Standards consensus judgment and rationale but they do not have rigorous failure related basis.

To demonstrate how the strain limits defined above from HBB are applied, the distribution of the normal strain across the cross-section of a beam under bending is considered. The comparison of the normal strain values to the 1%, 2% and 5% limits is illustrated in Figure 2.4.

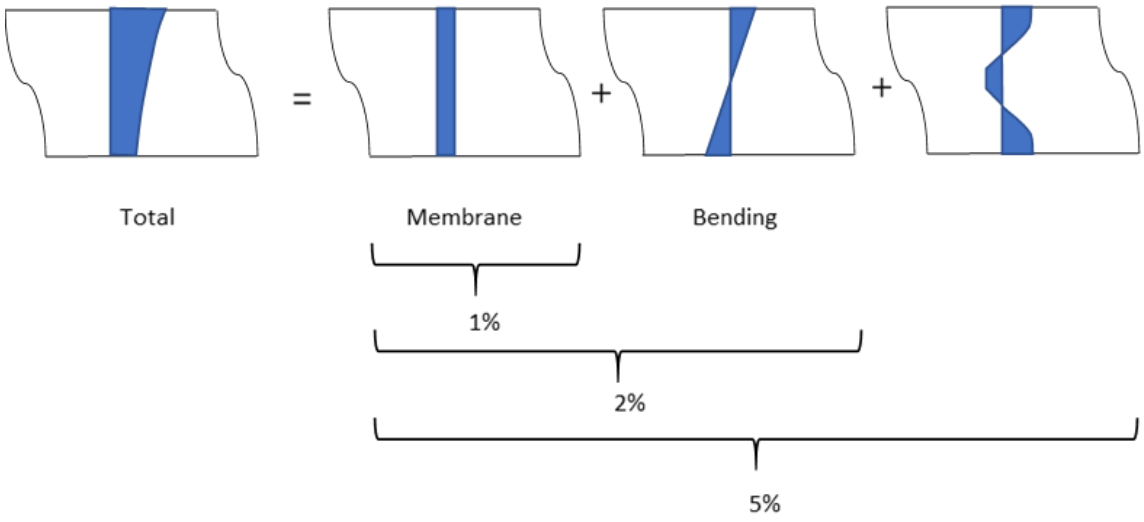

Figure 2.4. Illustration of the linearization procedure for the strain criteria in 1D

The linearization procedure for the three-dimensional distribution of accumulated inelastic strains over the cross-section is described below.

Strain linearization. The accumulated inelastic strains across a cross-section through the wall thickness of the structure, e.g., the ε_{yy} component of the accumulated inelastic strain shown in Figure 2.5, are subject to a strain linearization procedure, similar to that for the stresses, to determine the so-called accumulated membrane inelastic strains, $\varepsilon_{ij,m}$, and accumulated bending inelastic strain, $\varepsilon_{ij,b}$:

$$\varepsilon_{ij,m} = \frac{1}{t}\int_0^t \varepsilon_{ij}(x)dx \quad i,j = 1,2,3$$

$$\varepsilon_{ij,b} = \frac{6}{t^2}\int_0^t \varepsilon_{ij}(x) \times \left(\frac{t}{2} - x\right) dx \quad i,j = 1,2,3$$

where ε_{ij} are the three-dimensional accumulated inelastic strain components, and t is the wall thickness.

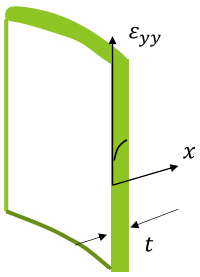

Figure 2.5. The distribution of the accumulated inelastic strain component, $\boldsymbol{\varepsilon_{yy}}$, through the wall thickness

To check the 1% strain limit for a cross-section of the structure, the principal strains are first computed from the accumulated membrane inelastic strains, $\varepsilon_{ij,m}$. Then the maximum positive value of the three principal strains is checked against the 1% strain criterion. If all three principal strains are negative, the 1% strain limit is considered met.

To check the 2% strain limit, the accumulated membrane and bending inelastic strains are first summed:

$$\varepsilon_{ij,mb} = \varepsilon_{ij,m} + \varepsilon_{ij,b}$$

Then the principal strains are computed from the new three-dimensional accumulated inelastic strains, $\varepsilon_{ij,mb}$. The maximum positive value of the so-computed principal strains is checked against the 2% strain criterion. Again, if all three principal strains are negative, the 2% strain limit is considered met.

For the 5% local strain limit, the principal strains from $\varepsilon_{ij}(x)$ for each point x on the cross-section along the wall thickness direction are first determined. Then the maximum positive value of the three principal strains is used to check against the 5% local strain criterion. This local strain limit is met if the 5% strain criterion is satisfied for all x in $0 \leq x \leq t$.

2.4.4.1.1 Strain limits check using elastic analysis result

There are a number of options for the strain limits check when the elastic analysis result is used. They are the A-1. A-2, A-3, B-1, B-2 and B-3 tests. All tests require stress linearization and stress classification. These options for the strain limits check are all based on the extension of the so-called Bree analysis which is captured by the Bree diagram in Figure 2.6.

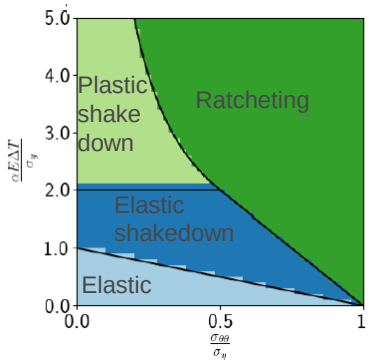

Figure 2.6. Bree diagram

Classical analytical analysis of the Bree cylinder provides bounds under biaxial pressure vessel loads. There are four regions delineated in the Bree diagram of Figure 2.6. They are

- Elastic region: all deformations are elastic
- Elastic shakedown region: deformation shakes down to elasticity
- Plastic shakedown region: deformation shakes down, but steady cycle includes plasticity
- Ratcheting region: strains continue to increase

The use of the tests A-1, A-2 and A-3 in article HBB-T-1320 is restricted within the "elastic" regime of the Bree diagram. The A-1 and A-2 tests check the strain limits compliance by

comparing the primary stress intensity and the secondary stress intensity range against certain prescribed limits, instead of evaluating the accumulated inelastic strains explicitly. The A-3 test is much more involved. It imposes restrictions on the creep deformation, essentially limiting it to be negligible. In fact, the A-3 test provides the criteria for the negligible creep regime where the small amount of creep deformation does not reduce the fatigue life at temperatures above the Code temperature limits of 700°F for ferritic materials and 800°F for austenitic materials.

The basic concept of the B-tests involves the following. If the structure does not ratchet there is a characteristic, average reference stress, or core stress, associated with the cycle that can be found from simple, analytic elastic-plastic analysis. Once the core stress is found, it can be used to compute the deformation over the design life using the isochronous stress-strain relations. The accumulated inelastic strains are evaluated, but using simplified bounding methods. The approaches employed in the B-tests are rather conservative. The satisfaction of the 1% strain criterion is considered adequate for the other two strain limits checks, and the 2% and the 5%, criteria are deemed satisfied without further evaluations.

The B-1 and B-2 tests in article HBB-T-1330 operate within the elastic shakedown and plastic shakedown regimes of the Bree-diagram. Design charts are provided in HBB-T-1330 to support the strain limits evaluation using either the B-1 or the B-2 test.

The B-3 test operates in the elastic shakedown, plastic shakedown and ratcheting regimes of the Bree-diagram. It starts with the accumulated strain values from Test B-1 and then corrects them for ratcheting and the extra creep deformation during relaxation above the core stress.

A summary of the characteristics of the A and B tests for conducting strain limits check using elastic analysis results is given in Table 2.8.

Table 2.8. Characteristics of simplified methods for strain limits

Test No.	Geometry/loading restrictions?	Cycle temperature restrictions?	Strain calculation?	Cycle definition
A-3	None	Entirely below creep range	None	Same as Division 1, Subsection NB
A-1	None	None	None	Whole life
A-2	None	Cold end below creep range	None	Whole life
B-2	None	Cold end below creep range	Core stress	Block
B-1	Either discontinuity or nonlinear temperature	Cold end below creep range	Core stress	Block
B-3	Either discontinuity or nonlinear temperature	None	Incremental summation	Individual

The B-3 test option has been removed from the 2021 Code edition of HBB due to the complexity of the procedure and the Code committee could not locate nor recreate the technical basis documents underlying the procedure.

2.4.4.2 Creep-fatigue check

The creep-fatigue check involves the evaluation of the combination of Level A, B, and C Service Loadings for accumulated creep and fatigue damage, including hold time effects. For a design to be acceptable, the creep and fatigue damage shall satisfy the following relation:

$$\sum_{j=1}^{p}\left(\frac{n}{N_d}\right)_j + \sum_{k=1}^{q}\left(\frac{\Delta t}{T_d}\right)_k \leq D$$

where

D = total creep–fatigue damage.

$(N_d)_j$ = number of design allowable cycles for cycle type, j, determined from one of the design fatigue curves corresponding to the maximum metal temperature occurring during the cycle. The design fatigue curves were determined from completely reversed loading conditions at strain rates greater than, or equal to, those noted on the curves.

$(T_d)_k$ = allowable time duration determined from the stress-to-rupture curves for a given stress and the maximum temperature at the point of interest and occurring during the time interval, k.

$(n)_j$ = number of applied repetitions of cycle type, j.

q = number of time intervals (each with a unique stress-temperature combination) needed to represent the specified elevated temperature service life at the point of interest for the creep damage calculation.

p = number of stress/temperature time histories.

$(\Delta t)_k$ = duration of the time interval, k.

For Division 5 applications, the creep-fatigue damage envelope is bilinear and it can be represented graphically as shown in Figure 2.7.

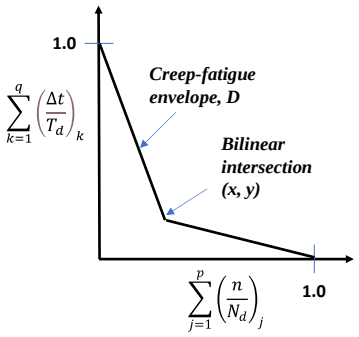

Figure 2.7. Creep-fatigue interaction diagram

The bilinear intersections for the Division 5 Class A materials are given in Table 2.9.

Table 2.9. Intersections of the bilinear creep-fatigue damage envelope for Class A materials

Material	Bilinear intersection (x, y)
Type 304 and 316 stainless steels	(0.3, 0.3)
Ni-Fe-Cr (Alloy 800H)	(0.1, 0.1)
2¼Cr-1Mo	(0.1, 0.1)
9Cr-1Mo-V	(0.1, 0.01)
Alloy 617	(0.1, 0.1)

Equivalent strain range determination. An equivalent strain range is used to evaluate the fatigue damage sum. Following Division 5, HBB-T-1413, the maximum equivalent strain range is determined using the history of the three-dimensional strain components within a cycle as follows. As noted subsequently, the treatment of peak strains arising from geometric discontinuities would depend on the analysis method employed.

Step 1. Divide the cycle period into time points.

Step 2. Select any time point as a reference time point, labeled as point o.

Step 3. For a time point i in the cycle, subtract the strains at time point o from the strains at time point i.

Step 4. Use these strain differences to determine an equivalent strain range $\Delta\varepsilon_{(equiv,i)}$ using

$$\Delta\varepsilon_{(equiv,i)} = \frac{\sqrt{2}}{2(1+v^*)}\left(\left(\Delta\varepsilon_{xi}-\Delta\varepsilon_{yi}\right)^2+\left(\Delta\varepsilon_{yi}-\Delta\varepsilon_{zi}\right)^2+\left(\Delta\varepsilon_{zi}-\Delta\varepsilon_{xi}\right)^2 + \frac{3}{2}\left(\Delta\gamma_{xyi}^2+\Delta\gamma_{yzi}^2+\Delta\gamma_{zxi}^2\right)\right)^{(1/2)}$$

$v^* = 0.5$ when using inelastic analysis results

$v^* = 0.3$ when using elastic analysis results

Step 5. Define $\Delta\varepsilon_{max}$ as the maximum value of the above calculated equivalent strain ranges for all time points associated with a reference point o, and for all possible reference time point within the cycle.

2.4.4.2.1 Creep-fatigue check using inelastic analysis results

When the inelastic analysis results are used to check the creep-fatigue compliance, the creep damage and fatigue damage evaluations are performed as follows.

Creep damage calculation. In the HBB creep-fatigue evaluation procedure, the creep damage, D_c, based on time fraction, may be determined using the integral form:

$$D_c = \int \frac{dt}{T_d}$$

For inelastic analysis the following equivalent stress, σ_e, is first determined:

$$\sigma_e = \bar{\sigma} exp\left[C\left(\frac{J_1}{S_S}-1\right)\right]$$

where $\bar{\sigma}$, J_1 and S_S are defined in terms of the principal stresses as

$$J_1 = \sigma_1 + \sigma_2 + \sigma_3$$

$$S_S = (\sigma_1^2 + \sigma_2^2 + \sigma_3^2)^{1/2}$$

$$\bar{\sigma} = \frac{1}{\sqrt{2}}[(\sigma_1 - \sigma_2)^2 + (\sigma_2 - \sigma_3)^2 + (\sigma_3 - \sigma_1)^2]^{1/2}$$

and the values of the material parameter C are given in Table 2.10.

Table 2.10. Values of C for equivalent stress

Material	Constant C
Type 304 and 316 stainless steels	0.24
Ni-Fe-Cr (Alloy 800H)	0.0
2¼Cr-1Mo and 9Cr-1Mo-V	0.16, if $J_1/S_S \geq 1.0$
	0.0, if $J_1/S_S < 1.0$
Alloy 617	0.24

When $C = 0$, the equivalent stress σ_e is reduced to the von Mises stress.

The allowable time duration, T_d, is determined by entering the rupture time-stress correlation at that stress value determined by dividing the equivalent stress σ_e at the location and time of interest by the factor, K'. The values of K' are given in Table 2.11.

Table 2.11. Values of K' for inelastic analysis

Material	K'
Type 304 and 316 stainless steels	0.67
Ni-Fe-Cr (Alloy 800H)	0.67
2¼Cr-1Mo	0.67
9Cr-1Mo-V	0.67
Alloy 617	0.67

Fatigue damage calculation. The fatigue damage is evaluated by entering a design fatigue curve at the strain range ε_t and the maximum metal temperature within the cycle. The strain range ε_t for the inelastic analysis is defined as $\varepsilon_t \equiv \Delta\varepsilon_{max}$ where $\Delta\varepsilon_{max}$ is determined as in Step 5 of the previous section.

Creep-fatigue compliance. The total damage D shall not exceed the creep-fatigue damage envelope as shown schematically in Figure 2.7 and in Table 2.9 for the bilinear intersection.

2.4.4.2.2 Creep-fatigue check using elastic analysis results

When elastic analysis results are used to assess the Code compliance on creep-fatigue, the following general requirements must first be met:

1. The primary stresses must meet the limit

$$P_L + P_b + Q \leq 3\bar{S}_m$$

   where $3\bar{S}_m$ is the creep shakedown limit, replacing $3S_m$.

2. Pressure induced discontinuity stresses and thermal induced membrane stresses are included as primary stresses.

The design parameter, $3\bar{S}_m$, is defined as:

$3\bar{S}_m = (1.5S_m + S_{rH})$ when only one extreme of the stress difference (that produces the maximum range of the primary plus secondary stress intensity, $P + Q$) occurs at a temperature above those covered by Division 1, Subsection NB rules; $(S_{rL} + S_{rH})$ when both extremes of the stress differences (that define the maximum range of $P + Q$) occur at temperatures above those covered by Division 1, Subsection NB rules.

S_{rH}, S_{rL} = relaxation strengths associated with the temperatures at the hot and cold extremes of the stress cycle. The hot temperature condition is defined as the maximum operating temperature of the stress cycle. The hot time is equal to the portion of service life when wall averaged temperatures exceed 800°F for austenitic alloys and 700°F for ferritic steels. The cold temperature is defined as the colder of the two temperatures corresponding to the two stress extremes in the stress cycle. The cold time is again equal to the portion of service life when wall averaged temperatures exceed 800°F for austenitic alloys and 700°F for ferritic steels.

Further, for using elastic analysis results for creep-fatigue check, the peak strains arising from geometric discontinuities are not included in the strain range evaluation. The creep-fatigue check consists of the evaluation of the total fatigue damage, the total creep damage, and the creep-fatigue interaction.

Fatigue damage calculation. The total fatigue damage, D_f, is obtained by summing the fatigue damages from different cycle types using the Miner's rule. The fatigue damage for each cycle type, $(n/n_d)_j$, is determined from the fatigue design curve, such as a typical one shown in Figure 2.8, by using an appropriate strain range from the cycle.

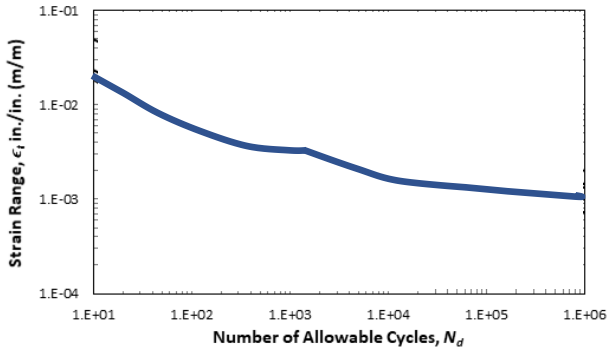

Figure 2.8. A typical fatigue design curve

Strain range determination. The determination of the strain range using the elastic analysis results is rather involved but the procedural steps are detailed in Division 5, HBB-T-1432. The basic evaluation process involves the calculation of an elastic effective strain range from elastic stresses and strains, and the correction of the elastic strain range to account for local plasticity, triaxiality and creep. The procedure uses primary + secondary stress range but without the peak stresses. The peak stresses are included through the stress concentration factors. This procedure also references the B-1 test for the strain limits check as this check needs to be passed first in order to prohibit ratcheting. However, the temperature anchor requirement in the B-1 test is not required as the creep-fatigue rules remove this condition.

Modification to the maximum equivalent strain range $\Delta\varepsilon_{max}$ calculated using the elastic analysis results is required to allow for the plasticity. There are three options to calculate the modified

maximum equivalent strain range, $\Delta\varepsilon_{mod}$, that accounts for the effects of local plasticity and creep. Option 1 is more accurate and hence less restrictive but requires iterative solution. Option 2 is the reference method, and option 3 is the simplest but most conservative. These three options are given as:

Option 1:

$$\Delta\varepsilon_{mod} = (K^2 S^* \Delta\varepsilon_{max})/\Delta\sigma_{mod}$$

Option 2:

$$\Delta\varepsilon_{mod} = \frac{S^*}{\bar{S}} K^2 \Delta\varepsilon_{max}$$

Option 3:

$$\Delta\varepsilon_{mod} = K_e K \Delta\varepsilon_{max}$$

where

$$K_e = 1, \text{if } K\Delta\varepsilon_{max} \leq 3\bar{S}_m/E$$

$$K_e = K\Delta\varepsilon_{max}/(3\bar{S}_m/E), \text{if } K\Delta\varepsilon_{max} > 3\bar{S}_m/E$$

with

$K =$ either the equivalent stress concentration factor, as determined by test or analysis, or, the maximum value of the theoretical elastic stress concentration factor in any direction for the local area under consideration.

$S^* =$ the stress indicator determined by entering the stress-strain curve of Figure HBB-T-1432-1 of Division 5 at a strain range of $\Delta\varepsilon_{max}$.

$\bar{S} =$ the stress indicator determined by entering the stress-strain curve of Figure HBB-T-1432-1 of Division 5 at a strain range of $K\Delta\varepsilon_{max}$.

$E =$ Young's modulus.

The creep strain increment, $\Delta\varepsilon_c$, for the stress cycle due to load-controlled stresses is determined by using a stress intensity equal to 1.25 times the effective creep stress $\sigma_c = Z \times S_y$ as defined in HBB-T-1332 of Division 5. The rules of HBB-T-1321, HBB-T-1331, and HBB-T-1332 apply to determining $\Delta\varepsilon_c$ except that the stress cycle time, including hold time between transients, shall be used instead of the entire service life. The restriction on Q_R in HBB-T-1323 relative to Table HBB-T-1323 does not apply to determining $\Delta\varepsilon_c$. Enter the isochronous stress-strain curves for the maximum metal temperature during the stress cycle time-temperature block with the $1.25\ \sigma_c$ stress held constant throughout each temperature-time block of the stress cycle. The $\Delta\varepsilon_c$ equals the sum of the creep strain increment accumulated in one stress cycle time.

Next, the multiaxial plasticity and Poisson ratio adjustment factor, K_v, is determined from:

$$K_v = 1 + f(K_v' - 1), \text{ but no less than 1}$$

where

$f =$ factor determined by entering Figure HBB-T-1432-2 of Division 5 at the Triaxiality Factor, T.F., for the stress state at each of the two extremes of the stress cycle. The larger magnitude of f shall be used.

K_v' = plastic Poisson ratio adjustment factor determined by entering Figure HBB-T-1432-3 at the ratio of $K_e K \Delta\varepsilon_{max}/(3\bar{S}_m/E)$

Finally, the total strain range, ε_t, that is used to enter the design fatigue curve is calculated as:

$$\varepsilon_t = K_v \Delta\varepsilon_{mod} + K\Delta\varepsilon_c$$

Creep damage calculation. In the HBB creep-fatigue evaluation procedure, the creep damage, D_c, is determined through a time-fraction calculation:

$$D_c = \sum_{k=1}^{q} \left(\frac{\Delta t}{T_d}\right)_k$$

There are two approaches available in HBB for the creep damage evaluation using elastic analysis results. The first is a general procedure where the stress relaxation profile is found by piecing together individual relaxation histories from individual cycles, assuming "full reset" behavior. The alternative procedure can be used if the following condition is met:

$$\varepsilon_t \leq 3\bar{S}_m/E$$

This would allow the use of one global relaxation history since the above condition precludes reverse plasticity during cycling. The stress relaxation profiles for these two approaches are illustrated in Figure 2.9.

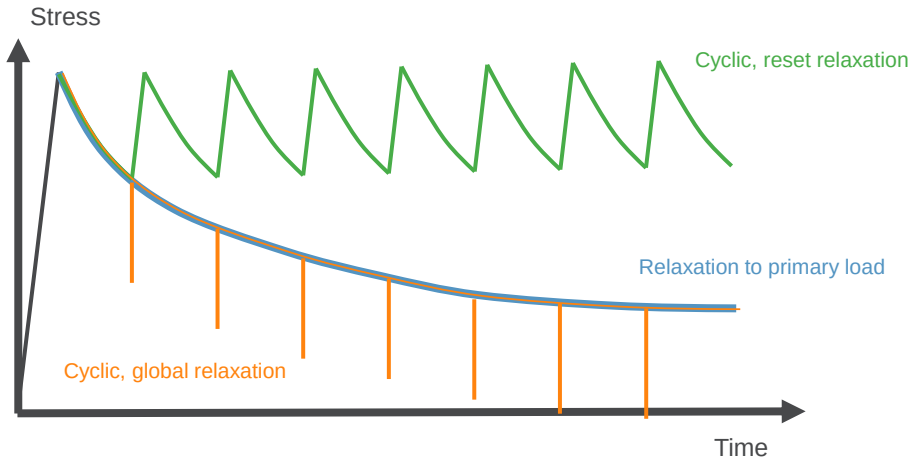

Figure 2.9. Two general approaches to the stress relaxation profile: full-reset behavior, and one global relaxation history

The general procedure. It consists of 10 steps and are detailed in HBB-T-1433(a). A high level description is given below. The calculations in steps 3 through 7 need to be repeated for each cycle type j.

Define average cycle time, $\bar{t}_j$, for each cycle type j:

Step 1. Define the total number of hours, t_H, above the code temperature boundary for HBB (700ºF for ferritic steels and 800ºF for austenitic alloys) for the entire specified service life.

Step 2. Define the local metal hold temperature, T_{HT}, during sustained normal operation.

Step 3. Define $\bar{t}_j \equiv t_H/n_j$, where n_j is the specified number of applied repetitions of cycle type j.

Step 4. Select time independent isochronous stress-strain curve corresponding to the temperature T_{HT}. This is also called the hot tensile curve.

Step 5. Account for stress relaxation during the average cycle time $\bar{t}_j$ and at a constant temperature, T_{HT}. The stress relaxation profile over the average cycle time is evaluated according to, Figure 2.10,

$$S_r = S_j - 0.8G\left(S_j - \bar{S}_r\right)$$

where

S_r = relaxed stress level at time t adjusted for the multiaxial stress state

S_j = the initial stress level for cycle type j

$\bar{S}_r$ = relaxed stress level at time t based on a uniaxial relaxation model

G = the smallest value of the multiaxiality factor as determined for the stress state at each of the two extremes of the stress cycle. Any value of G greater than 1.0 shall be taken as 1.0. The multiaxiality factor is defined in terms of the principal stresses as

$$\frac{\sigma_1 - 0.5(\sigma_2 + \sigma_3)}{\sigma_1 - 0.3(\sigma_2 + \sigma_3)}$$

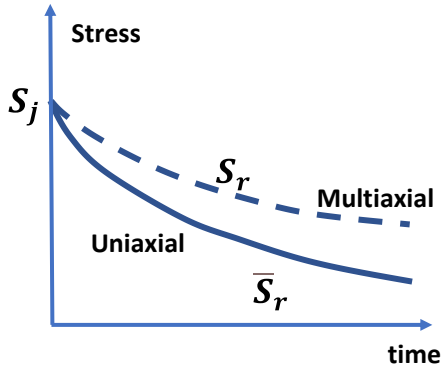

Figure 2.10. Multiaxial relaxation calculated from uniaxial relaxation

An alternative stress relaxation evaluation procedure for Step 5 using the isochronous stress-strain curves is provided in Division 5, HBB-T-1433.

Step 6. Define the transient load-controlled stresses, S_{TRAN}, and transient time, t_{TRAN} as illustrated in Figure HBB-T-1433-3 of Division 5, and modify the stress-strain history if there is load-controlled transient effect.

Step 7. Define cycle transient temperature, $(T_{TRAN})_j$. In no case shall $(T_{TRAN})_j$ be defined as less than the hold time temperature, T_{HT}. Note that $(T_{TRAN})_j$ is only used in the creep damage evaluation but not in the stress relaxation evaluation.

Step 8. Repeat steps 3 to 7 for all cycles and superimpose. The superposition is illustrated in Figure HBB-T-1433-4 of Division 5.

Step 9. Divide composite stress-time history into q time intervals of time of constant stress $(S)_k$ and constant temperature $(T)_k$.

Step 10. For each time interval $(\Delta t)_k$, obtain the allowable time duration, $(T_d)_k$ from the expected minimum stress-to-rupture curve in Figure HBB-I-14.6 of Division 5, using the temperature $(T)_k$ and the appropriate stress of $(S)_k/K'$ where K' is given in Table 2.12.

Table 2.12. Values of K' for elastic analysis

Material	K'
Type 304 and 316 stainless steels	0.9
Ni-Fe-Cr (Alloy 800H)	0.9
2¼Cr-1Mo	0.9
9Cr-1Mo-V	1.0
Alloy 617	0.9

It is noted that the creep-fatigue damage evaluation procedure based on elastic analysis results described in these subsections is only applicable up to 1200ºF for Alloy 617. For temperatures higher than 1200ºF, the elastic, perfectly plastic creep-fatigue evaluation method described in Division 5, Code Case N-898 is required.

The alternative procedure is described in detailed in HBB-T-1433(b) of Division 5.

2.4.4.3 Buckling check

Section III, Division 1, paragraph NB-3133 provides the buckling limits for specific geometrical configurations under specific loading conditions in low temperature service. Section III, Division 5 Article HBB-T-1500 considers the effects of creep due to long term loadings at elevated temperatures. The HBB-T-1500 limits are applicable to general configurations (geometries) and address time-independent behavior as well as time time-dependent creep behavior of the material.

Two different categories of buckling are considered in HBB-T-1500. Load-controlled buckling is characterized by continued application of an applied load in the post-buckling regime, leading to failure. Strain-controlled buckling is characterized by the immediate reduction of strain-induced load upon initiation of buckling, and by the self-limiting nature of the resulting deformations.

In the time-independent buckling regime and for general configurations, the HBB-T-1500 limits are specified in terms of load factors for load-controlled buckling and strain factors for strain-controlled buckling. They are specified for Design Loading, Service Loading and Test Loading. If strain-controlled and load-controlled buckling interact, or if there is significant elastic follow-up, the load factors applicable to load-controlled buckling shall be used. For load-controlled buckling, the initial imperfections and tolerances shall be considered, but they need not be considered for pure strain-controlled buckling. Also, buckling analysis shall be based on expected minimum stress-strain curves.

For the time-dependent regime, only load factors for load-controlled buckling, and Service Loadings only, are specified. They are shown in Table 2.13. The designer shall demonstrate that buckling will not occur during the specified lifetime for a load history obtained by multiplying the specified Service Loadings by the corresponding factor given in Table 2.13. Strain factors for strain-controlled buckling in the time-dependent regime are not required because strain-controlled loads are reduced concurrently with resistance of the structure to buckling when creep is significant.

Table 2.13. Time-dependent load-controlled buckling factors.

Service Loadings	Load Factors
Level A	1.5
Level B	1.5
Level C	1.5
Level D	1.25

In the time-dependent regime, article HBB-T-1500 also provides time-temperature limits for sphere under external pressure and cylinder under axial compression, and temperature limits for cylinder under external pressure. For temperatures below these limits, the design limits of Division 1, NB-3133 or the time-independent load and strain factors of Division 5, HBB-T-1521 may be applied without the consideration of creep effects.

2.4.5 Bolts

2.4.5.1 Load-controlled limits.

There are only three permissible bolt materials in Division 5. They are Type 304 and 316 stainless steels and Alloy 718. The bolting allowable stress is half (½) that of the base metal. In terms of the relative strength, the allowable stress for Alloy 718 is about five times that of Type 304 and 316 stainless steels at 550ºC.

For the Design Conditions limits, the rules for bolts are the same as that in Division 1, Subsection NB, but with high temperature allowable stress. Guidance is provided in HBB-3232 of Division 5 when gaskets are used (for preservice testing only.)

For Service Level A and B, the average stress due to pressure is limited to the allowable stress S_{mt}. The maximum values for service stresses (averaged across the bolt cross section and neglecting stress concentrations), such as those produced by a combination of preload, pressure, and thermal expansion, are limited to two times $(2\times)$ of S_{mt}. The use fraction is limited to 0.5 for multiple loading conditions.

The maximum linearized service stress at the periphery of the bolt cross section, resulting from tension-plus-bending and neglecting stress concentrations, is limit to three times $(3\times)$ of S_{mt}. The use fraction is limited to 0.67 for multiple loading conditions.

For Service Level C and D, the above limits only apply to primary loads in bolts.

2.4.5.2 Deformation-controlled limits

The strain limits and creep-fatigue criteria for bolts are the same as the base metal. Additional requirements are as follows.

Unless it can be shown by analysis or tests that a lower fatigue strength reduction factor and/or a lower stress rupture reduction factor is appropriate, the reduction factors shall be not less than 4.0 and 1.8, respectively, for the threaded region.

The geometrical restriction of the thread and fillet radii at the end of the shank as described in Section III Appendices, Mandatory Appendix XIII, XIII-4230(b)(2) and XIII-4230(b)(3) shall apply.

2.4.6 Inelastic analysis methods

The general guidance for inelastic analysis methods provided in HBB-3214.2 of Division 5 is rather limited. The features of constitutive equations that are important for the evaluations of Division 5 structural failure modes are:

- Effects of plastic strain hardening, including cyclic loading effects and hardening or softening at elevated temperatures
- Primary creep and the effects of creep strain hardening as well as softening due to reverse loadings
- Effects of prior creep on subsequent plasticity and vice versa

Generally, it is appropriate to use average (or nominal) stress, strain and creep data, except for buckling and instability inelastic analyses which should be based on minimum behavior. Unified constitutive equations which do not distinguish between rate-independent plasticity and creep are more appropriate for 9Cr-1Mo-V, particularly at higher temperatures.

More comprehensive discussions were provided in a series of Welding Research Council bulletins on recommended practices [6]. A detailed technical basis can be found in DOE/RDT Standard F9-5T.

The 2021 edition of Division 5 does not provide reference inelastic models for any of the Class A materials. Specification of the material model is left to owner's Design Specification or designers. This limits the application of the inelastic analysis methods for Division 5 Code compliance checks. Historical experience on the design of the Clinch River Liquid-Metal Breeder Reactor showed that inelastic analysis was the least over-conservative of the Division 5 design evaluation options. It was necessary in critical locations where design by elastic analysis is too conservative to produce a realizable design.

As previously described, a new Appendix HBB-Z is being introduced to Division 5, through ASME C&S RC 19-317, where guidance is provided on the construction of suitable inelastic models from data. A reference unified viscoplastic constitutive model for 9Cr-1Mo-V for Division 5 applications is also included in the new appendix. Unified viscoplastic constitutive models for Type 316 stainless steel and Alloy 617, developed under the U.S. Department of Energy funding support, will be submitted for approval for Division 5 Appendix HBB-Z by end of 2021. Development of the inelastic model for Alloy 800H will follow.

2.4.7 Design Parameters

To execute the design checks described in the previous sections, material specific design parameters covering different temperatures and times are required. They are:

Allowable stresses

S_m: time-independent allowable stress; based on yield and ultimate strengths from tensile tests at temperature

S_t: time-dependent allowable stresses; based on data from creep rupture tests

S_r: time-dependent expect minimum stress-to-rupture; based on data from creep rupture tests

S_{mt}: allowable stress for Service Level primary load check; equal to the lesser of (S_m, S_t)

S_0: allowable stress for Design Condition primary load check, equal to the lesser of ($S, S_{mt}@300{,}000h$)

R: Stress rupture factor (for welds) used in conjunction with S_r for the base metal to determine the rupture stress for weld metal; based on data from creep rupture tests of weld metal or weldment and base metal

Thermal aging factors

These factors are applied to the temperature-dependent yield strength, S_y, and tensile strength, S_u, to account for the potential strength reductions due to extended thermal exposures during plant operations. These reduced strengths are only used in the allowable stresses S_m and S_{mt} when conducting the primary load checks.

Isochronous stress-strain curves

These curves represent the cross-plots of stress versus strain for a given temperature and time based on the nominal total strain equation under the creep condition. The strain equation is obtained from uniaxial tensile data and creep data. These curves are used for the checks on deformation-controlled acceptance criteria.

Fatigue design curves

These design curves are used to calculate the fatigue damage in the creep-fatigue design check. The curves are based on data from strain-controlled cycling tests at a relatively high strain rate, e.g., 10^{-3} per second. The high strain rate is employed in order to suppress the creep effects on cycles to failure. It is because the Division 5 creep-fatigue procedure accounts for creep damage under creep-fatigue cycling separately. Thus, fatigue design curves generated with slower strain rate will contain additional creep effect that has already been accounted for in the creep damage evaluation.

Creep-fatigue interaction diagram

This provides the creep-fatigue damage envelope for the creep-fatigue check. The envelope is bilinear and constructed using data from strain-controlled cyclic tests with hold times at maximum and/or minimum strain level. The envelope is intended to represent the nominal behavior of creep-fatigue interaction. The source of conservatism is endowed in other steps of the creep-fatigue evaluation procedure.

The temperature ranges and/or time durations of the temperature and time-dependent design parameters provided in Division 5 and its code cases for the Class A base metals are shown in Table 2.14 and Table 2.15.

Table 2.14. Temperatures and time ranges of design parameters for base metals – List 1

Base Material	S_t, S_{mt}, S_r, temperature range and max. time	Thermal aging factors for S_y and S_u , temperature range and max. exposure time
Type 304 stainless steel	>800 to 1,500F; 300,000h	≥900 to 1,500F; 300,000h
Type 316 stainless steel	>800 to 1,500F; 300,000h	>900 to 1,500F; 300,000h
Ni-Fe-Cr (Alloy 800H)	S_t, S_{mt}: >800 to 1,400F; 300,000h S_r: >800 to 1,650F; 500,000h	>1,350 to 1,400F; 300,000h
2¼Cr-1Mo	>700 to 1,100F; 300,000h >1,100 to 1,200F; 1,000h	>800 to 1,100F; 300,000h >1,100 to 1,200F; 1,000h
9Cr-1Mo-V	>700 to 1,200F; 300,000h	>900 to 1,200F; 300,000h
Alloy 617	>800 to 1,750F, 100,000h	>800 to 1,750F; 100,000h
SA533B, SA508 pressure vessel steels	S_t, S_{mt}: >700 to 800F; 3,000h (Service Level B) >800 to 1,000F; 1,000h (Service Level C or D) S_r: >700 to 1,000F; 100,000h	Not used

Table 2.15. Temperatures and time ranges of design parameters for base metals – List 2

Base Material	Isochronous stress-strain curves, temperature range and max. time	Fatigue design curves, max. temperature
Type 304 stainless steel	800 to 1,500F; 300,000h	1,300F
Type 316 stainless steel	800 to 1,500F; 300,000h	1,300F
Ni-Fe-Cr (Alloy 800H)	800 to 1,400F; 300,000h	1,400F
2¼Cr-1Mo	700 to 1,100F; 500,000h (2019 edition) 1,100 to 1,200F; 1,000h	1,000F
9Cr-1Mo-V	700 to 1,200F; 300,000h	1,200F (2021 edition)
Alloy 617	800 to 1,750F, 100,000h	1,750F
SA533B, SA508 pressure vessel steels	700 to 1,000F; 1,000h	1,000F

The coverage on bolt materials is shown in Table 2.16.

Table 2.16. Temperatures and time ranges of design parameters for bolt materials

Bolt Material	S_{mt}, temperature range and max. time	Fatigue design curves, max. temperature
Type 304 stainless steel	>800 to 1,300F; 200,000h	1,300F
Type 316 stainless steel	>800 to 1,300F; 200,000h	1,300F
Alloy 718	>800 to 1,050F; 300,000h	Fatigue curve not provided

2.4.8 Conditions on allowable stresses in Division 5, 2017/2019 edition

As described previously the USNRC is reviewing ASME Section III, Division 5, 2017 edition, for endorsement. However, revisions of some of the allowable stresses and design parameters have been made in the 2019 edition and the to-be-issued 2021 edition. Further, there are revisions targeted for actions in the 2023 edition. An assessment was made by Sham [7] on the values of the allowable stresses in the 2017/2019 edition of Division 5, judged to provide a reasonable assurance of adequate protection, where applicable, are provided. The results are summarized in Table 2.17.

Table 2.17. Max. temperature conditions on allowable stresses

Base Material	S_{mt}, S_{r}, conditions on max. temperature	Applicable Code edition
Type 304 stainless steel	Restricted up to 1,300F	2017 and 2019
Type 316 stainless steel	Restricted up to 1,300F	2017 and 2019
Ni-Fe-Cr (Alloy 800H)	No restrictions	2017 and 2019
2¼Cr-1Mo	Restricted up to 950F	2017 and 2019
9Cr-1Mo-V	No restrictions	2019
Alloy 617	No restrictions	Code Case N-898
SA533B, SA508 pressure vessel steels	No restrictions	2017 and 2019

3 Design and Construction of Welded Components

3.1 Creep failure of weldments in high temperature service

Experimentally, overmatched weldments considering time-independent strength – weld/filler/base material combinations that are stronger than the base material in, for example, a standard tension test – are often undermatched when considering long-term creep rupture [8]. Typically, a combination of detrimental microstructural changes caused by the weld heat input in the base metal in the heat affected zone and the metallurgical notch effect caused by differences in the weldment and base material creep deformation combine to cause this reduction in the rupture strength [9]. The design and construction of high temperature nuclear components must account for the potential weakness of the welds compared to the component base material.

Figure 3.1 is a schematic of a weldment showing the weld material, the Heat Affected Zone (HAZ) of the base material, and the transition to undistributed base metal. Experimentally, failure often occurs in the HAZ rather than the weld or base metal proper, suggesting the root cause of weldment failure at high temperatures are microstructural changes to the base material caused by the weld heat. Oftentimes, a weld modeling framework divides the HAZ into coarse-grained, fine-grained, and intercritical zones with different properties, as shown in the figure.

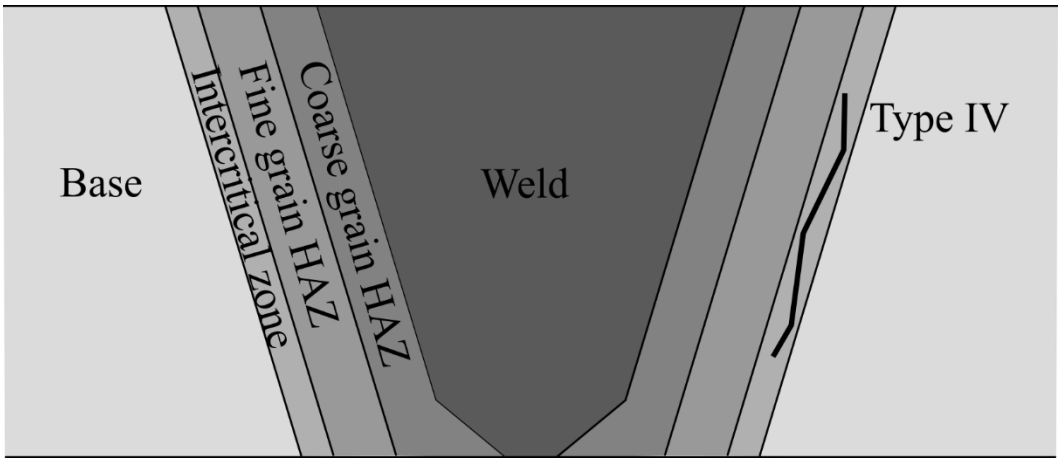

Figure 3.1. Schematic of a weldment illustrating the Coarse-grained Heat Affected Zone (CHAZ), Fine-grained Heat Affected Zone (FHAZ) and the intercritical region, along with the weld and undisturbed base metal. The figure shows the location of a Type IV crack

Two effects contribute to the decreased strength of weldments in a structure operating at high temperatures. The first is that weldment material, particularly the base metal in the heat affected zone, often deforms differently than the unaffected base metal [10], [11]. The differences in the HAZ creep deformation can be subtle – for example, some work suggests the fine grained and coarse grained HAZs can have very different creep deformation laws [12]–[14]. Regardless, the net effect of the difference in creep deformation between weldment and base material is to concentrate deformation and damage into the weldment. The weld acts like a physical notch, hence the "metallurgical notch effect" referenced in design codes.

The second effect is a decrease in the creep resistance of the weldment when compared to the base metal. This decrease may be attributed to the weld material but, again, more often it occurs in the

HAZ. The mechanisms causing a decrease in creep resistance vary with the material, but the heat input from the welding process can cause changes to the base material grain size and shape distribution, the dislocation density, and the precipitate structure. All these microstructural changes can in turn affect the material creep resistance.

It is difficult to dissociate the notch effect from a decrease in the weldment creep resistance. Cross-weld creep tests, described in greater detail below, examine the net effect of both differences in weldment creep deformation and creep resistance on the overall creep rupture life of a weldment.

Weld failure mechanisms are often categorized by their location in the idealized structure of a weldment (Figure 3.1) or the loading condition causing weld failure. This categorization scheme ignores the microstructural causes of failure, which could conceivably be different for different materials even for the same failure type. There are two prominent mechanisms affecting the materials allowed for high temperature nuclear construction in the ASME Boiler Code.

Type IV cracking often occurs in Cr-Mo ferritic steels in components operating in the creep range. This failure mechanism is described by its location in the HAZ, in the intercritical region between the fine-grained HAZ and the base metal [15]. Materials of interest to this report include 2.25Cr-1Mo (Grade 22) steel and modified 9Cr-1Mo-V steel (Grade 91).

Most researcher attribute Type IV to over-coarsening of strengthening precipitates in the intercritical zone [16], [17]. There is widespread agreement that better post-weld heat treatments may improve the performance of the weldment and some suggestion that the addition of boron to the alloy chemistry may reduce its susceptibility to Type IV cracking. Type IV cracking is a time dependent failure mechanism, reducing the rupture strength of the weldment when compared to base material but typically not associated with any particular loading event. Type IV cracking is then the prime example of a failure mechanism dealt with in the ASME Section III, Division 5 design code through weld stress rupture factures, described in greater detail below.

The second mechanism of interest is reheat cracking, also called stress relief cracking, stress relaxation cracking, or post weld heat treatment cracking [18], [19]. Failure is typically intergranular and occurs in the coarse grained HAZ. This mechanism is most common in thick-walled austenitic stainless steel sections [20], [21] though the mechanism can occur in ferritic steels like Grade 22 [22].

As the name suggests, these cracks often appear during a post weld stress relief heat treatment. This suggests that the cracking mechanism is related to the relaxation of the weld residual stress [23]. In particular, cracking is thought to occur when the weldment does not have sufficient ductility to fully relax out the initial weld residual stress. For untreated or improperly heat-treated welds the cracking may be deferred to after the start of operation, though it typically occurs during the first few loading cycles. For components operating in the creep range, the initial few cycles essentially serve as an impromptu stress relief heat treatment.

This mechanism is essentially time-independent – it occurs early in the component service life and does not explicitly represent a reduction in the creep rupture strength of the weldment. It has to do with creep deformation only to the extent that creep is the mechanism causing stress relief in

the weldment. As such, this is an example of a mechanism dealt with by the Section III, Division 5 construction rules.

3.2 ASME Section III, Division 5 rules

Section III, Division 5 contains design, fabrication, and inspection rules for welded components operating in high temperature nuclear service. Many of the Division 5 criteria refer back to Section III, Division 1 rules for nuclear service below the creep range for the basic requirements. However, Division 5 supplements these basic rules with specific provisions for high temperature service.

A full summary of the base Division 1 rules is beyond the scope of this report. As described in subsequent sections, the *design* rules in Division 1 are largely supplanted by Division 5 criteria. This leaves the Division 1 rules to form the basis of the *construction* and *inspection* requirements for weldments in Division 5. In turn, the Division 1 rules build on the criteria in Section IX of the ASME Boiler and Pressure Code, supplementing these non-nuclear commercial rules with additional criteria as appropriate. This report focuses on the Division 5 criteria specific to high temperature nuclear service.

Section III, Division 5 requires overmatched welds for time-independent material properties and allowable stresses – i.e. the yield strength and tensile strength of the weldment should exceed the corresponding base material properties. However, as described above, this condition does not necessarily produce an overmatched weldment when considering time-dependent failure.

The basic experimental data used by the Division 5 design rules are weld stress rupture factors (R). These are time- and temperature-dependent factors expressing the reduction in the creep rupture strength of a weldment, of a particular type, compared to corresponding base material. In effect, the product of $R \times S_r$, with S_r the minimum strength to rupture of the base metal, gives the minimum creep rupture strength used by Division 5 in the design of a weldment.

Several factored material properties feed into the allowable stress S_{mt} used in Division 5 for base material design – yield strength, tensile strength, creep rupture strength, and creep deformation criteria. However, the allowable stress specific to weld material only considers the minimum stress to rupture. When the design rules require a weld allowable stress the Code uses the minimum of the base material allowable stress and $0.8 \times R \times S_r$ where the factor of 0.8 corresponds to the base material allowable stress criteria of 80% of the minimum stress to rupture.

This definition of the weld allowable stress does not include weld-specific time independent strength or creep deformation properties, though the criteria does bound the weld allowable stress with the base material properties if they control over the criteria $0.8 \times R \times S_r$. Neglecting the time independent strength in the weld allowable stress definition is conservative as the welds allowed by Division 5 are overmatched for time independent failure. Neglecting the creep deformation criteria contributing to the base material allowable stress reflects the limited availability of weldment-specific creep deformation testing.

HBB-Y-2300 describes the experimental data required to qualify a weld for high temperature service using the Section III, Division 5 rules. The primary additional data, beyond the tests required

to qualify the weldment for low temperature service, are cross-weld creep rupture tests. The stress rupture factors R for the weldment are constructed from a database of experiments of this type.

Figure 3.2 describes a cross-weld creep test. Unlike base metal creep tests (ASTM standard E139 [24]) there is no accepted experimental standard. However, the approach has been described in the literature since at least the 1980s [25] with a great deal of development in the 1990s [26], [27]. The key point is that the specimens are machined so that specimen gauge encompasses the entirety of a qualified weldment: weld metal but also the heat affected zone on either side of the weld itself. This ensures the rupture data accounts for any degradation in the base material strength caused by the thermal history of the HAZ, for example due to Type IV cracking.

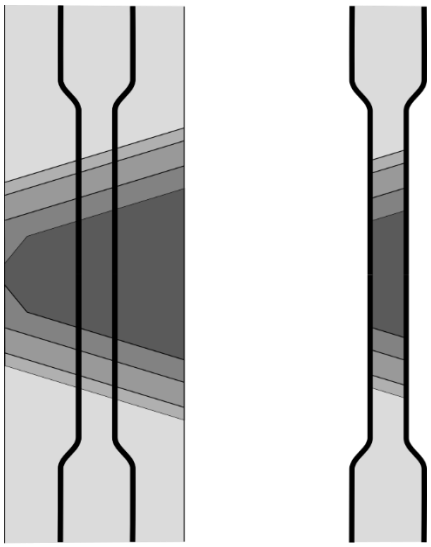

Figure 3.2. Schematic of a cross-weld creep specimen. (a) shows how the specimen might be machined from a V-groove full penetration butt weld. The colors in the figure indicate the weld metal, CHAZ, FHAZ, intercritical zone, and base metal. (b) demonstrates the machined sample contains the entire weldment – weld, HAZ, and undisturbed base – in the sample gauge.

Some of the early weld creep data used to generate the rupture factors in Division 5, particularly for austenitic stainless steel, were based on weld metal creep tests – not cross-weld tests [9]. The transition from weld metal to cross-weld creep tests occurred sometime in the 1980s and was likely a response to HAZ failure in Grade 91 steel and other ferritic alloys. While this is predominantly a historical limitation – the current ASME position is that the reduction factors should be based on cross-weld tests – for the austenitic steels in particular basing the reduction factors on weld-only creep test data remains reasonable. These alloys are less susceptible to metallurgical changes in the HAZ causing failure when compared to ferritic steels like Grade 91. For example, properly

welded austenitic materials are less susceptible to Type IV cracking [15] as compared to ferritic alloys.

The stress rupture factors (R) are generated from a database of cross-weld creep rupture tests. The ASME approach is to calculate the ratio of the *average* cross-weld stress to rupture to the *average* base metal stress to rupture:

$$R = \frac{\sigma_R^{weld}(T,t)}{\sigma_R^{base}(T,t)}$$

where both the base and weld rupture strength depend on both temperature and time. Figure 3.3 illustrates the process. Typically, a Larson-Miller fit extrapolates the experimental data for base weld and base rupture strength out in time to reduce the required test time, as shown on the figure. This approach means that, in general, the stress rupture factors R, listed in Division 5 depend on temperature and time. Furthermore, based on the overmatched weld principal, in general the reduction factors are 1.0 for short times and decrease as time increases. The exception to both these rules are the rupture factors for Grade 91 steel, discussed in detail below.

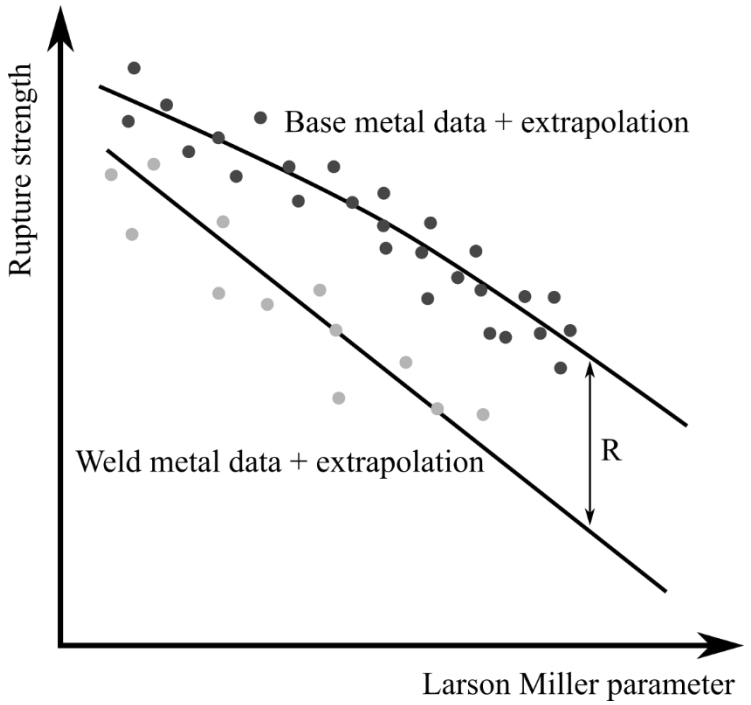

Figure 3.3. Schematic demonstrating the calculation of the weld stress rupture factor as the ratio of an extrapolated model for the weld average stress to rupture to the base metal average stress to rupture.

Section III, Division 5 Nonmandatory Appendix HBB-Y describes the data required to develop the Division 5 rupture factors and qualify a new weld type for high temperature service. The appendix states that the weld type must be defined by providing:

(a) Identification of the types of joints
(b) Identification of the weld processes
(c) Identification of filler metals and composition
(d) Identification of the weld qualification procedures

(e) Postweld heat treatment
(f) Delta ferrite determination
(g) Time-independent data corresponding to the data required for wrought materials (tensile tests providing temperature-dependent values of the yield and ultimate tensile strengths)
(h) Stress rupture data from cross-weld specimens

Items (a) to (e) in this list identify the weld type, the data from (g) confirms the weld time-independent properties are overmatched, and the data from (h) establishes the time- and temperature-dependent rupture factors.

Additionally, HBB-Y recommends a few weld creep-fatigue tests to validate that the very conservative adjustments to the creep-fatigue acceptance criteria for welds (described below) remain adequately conservative for the new weldment.

3.2.1 Class A components

Section III, Division 5, Subsection HB, Subpart B describes the design and construction of Class A components in high temperature service. These rules are the most critical in Division 5 as:

1) They form the basis of the rules described in several of the other subsections of the Code (for example the Core Support rules in Subsection HG, Subpart B.
2) They apply to the most safety-critical components.

As such this report describes the HBB rules in detail and then briefly summarizes the remaining weld rules.

HBB only allows a limited number of weld electrode/weld material/base material. Only welds listed in Table HBB-I-14.1(b) with stress rupture factors listed in Tables HBB-I-14.10A-E can be used in Class A construction. Section 3.3 analyzes these allowable welds for time/temperature gaps and other potential shortcomings. The allowable weld combinations are described in detail by references to the base metal, the filler specification (SFA), and the particular electrode type.

The weld rupture factors in these tables for fixed temperature start at 1.0 and decrease as time increases, reflecting an increasing degradation of the weld strength for longer exposure to high temperatures and creep deformation. Similarly, the factors tend to go to 1.0 as temperatures decrease below the creep range, reflecting the Code philosophy of overmatched weldments.

Grade 91 is currently an exception – the current Code weldment stress rupture factors in the 2019 of the Code depend only on temperature and not on time. This reflects the limited understanding of Type IV cracking mechanisms in Grade 91 at the time the current Code factors were drafted. Current work in the ASME Code Committees modernizes these factors by providing time-dependent values. The gap analysis section, below, describes this work in greater detail.

In addition to the design, construction, and inspection requirements described below, HBB-2430 provides additional acceptance criteria for delta ferrite content of weld consumables and backing material. Delta ferrite is a second phase present in stainless steel. Delta ferrite contributes to material strength and so a certain delta ferrite content is required to develop adequate high temperature material properties [28]. However, too much delta ferrite causes time-temperature dependent microstructural changes leading to embrittlement, which can cause hot cracking [29]. As

such, the HBB rules provide both a lower and upper limit on delta ferrite concentration for components in high temperature service. Specifically, the weld materials must have a Ferrite Number (FN) between 3 and 10. Additionally, the Code rules specify the method of measuring the FN and provide exclusions for certain types of weld consumables.

Dissimilar metal welds are allowed in Class A construction but HBB-3123 and HBB-3139.1 warn that the design of dissimilar metal joints at high temperatures is especially challenging because of mismatches in the coefficient of thermal expansion. The Code does not provide design rules for dissimilar metal joints, leaving these types of connections to be qualified by direct component testing.

3.2.1.1 Design

The basic design approach in HBB is to analyze the welds as if they have base material properties but the actual geometry of the as-welded configuration and apply more conservative acceptance criteria to the weldment regions. In practice this means that (generally) the allowable stresses for weldments are less than those for base metal and similarly the strain accumulation and creep-fatigue acceptance criteria for weldments are more stringent than for base metal.

Per HBB-3139.2 welds in Class A components must comply with the rules in Section III, Division 1, NB-3350. The weld design rules in HBB supplement this low temperature criteria, except that where there is a conflict the particular high temperature rules in HBB control over the low temperature rules in NB.

For primary load design, stresses in the welds are calculated using an elastic analysis, treating the weld material as if it had base material elastic properties. The stresses in the component, including in the welds, are classified to determine the primary stresses and linearized to divide the primary stress into membrane and bending contributions. The stress intensity of these membrane and bending stresses are then assessed against the primary load allowable stresses (either individually or in combination).

As described in the previous chapter, HBB has two separate primary load checks using two different types of loading. In the Design Limits checks the welds are entirely neglected – they are analyzed as base material and the stresses compared against the base metal allowable stress S_o.

For the Service Loading check the weld stresses are compared to reduced allowable stresses. As with base metal, these allowable stresses vary depending on the category of the Service Load. In all cases the weld allowable stresses are bounded by the base metal allowable stresses – if the base metal allowable stresses are lower than the weld allowable stresses the base metal allowable stresses control.

For Service Levels A and B the weld check replaces the allowable stress S_{mt} by the lesser of the base metal S_{mt} and the quantity $0.8S_r \times R$, where S_r is the base metal minimum stress to rupture.

Similarly, the weld check replaces the allowable stress S_t with the lesser of the base metal S_t and the quantity $0.8S_r \times R$.

For Service Level C in weldments a similar substitution occurs replacing the allowable S_t with the lesser of the base metal allowable stress S_t and the quantity $0.8S_r \times R$.

For Service Level D weld and base metal have the same allowable stresses, as the allowables are based on time-independent properties for this category of loading. Note the general principle holds for all the primary stress criteria: the weld time-independent properties match the base metal while the time-dependent properties may be reduced by the weld stress rupture factor. This reflects the general principal of overmatched weldments.

Replacing S_t with the quantity $0.8S_r \times R$ in the weld allowable stress definition is a compromise. The full definition of S_t for base metal includes criteria on the material time-to-tertiary creep and the time to accumulate 1% creep strain, in addition to criteria based on the minimum stress to rupture. Deformation data is seldom available for weldments and so the Code only applies a weld-specific factor to the rupture stress.

The strain limits and creep-fatigue criteria apply a similar modification for welds. For both the design by elastic analysis and design by inelastic analysis options in Nonmandatory Appendix HBB-T weldments are analyzed as if they were base metal. However, the strain accumulation limit for weldments (defined as the weld metal extended out by 3 times the section thickness in each direction) is half that of base metal, i.e. the lesser of:

- 0.5% average strain
- 1% linearized bending strain
- 2.5% maximum strain

For creep-fatigue, the number of allowable design cycles for the fatigue damage calculation are halved for weld material. That is, in the fatigue damage calculation damage in a weldment is calculated as

$$D_f = \sum \frac{N_i}{0.5N_f(\Delta\varepsilon_i)}$$

where N_f is the number of design cycles to failure for base metal for the given strain range. In the creep damage calculation damage in a weldment is calculated using the base metal minimum stress to rupture modified by the weld stress rupture factor R. The designer uses the unmodified base metal creep-fatigue interaction diagram as the acceptance criteria for welds.

One critical aspect of implementing these strain accumulation and creep-fatigue rules is that the stress analysis must represent the actual weld geometry (see Figure 3.4). HBB-3353 explicitly describes this requirement. Generally, this means that HBB encourages designers to require welds to be ground flush. Though the construction rules do allow as-deposited welds (see HBB-4424), it is essentially impossible to include the actual weld geometry in the initial design analysis, as it will be unknown until component fabrication. In contrast, if the welds are ground flush the initial design can include the correct geometry, per the Code requirements.

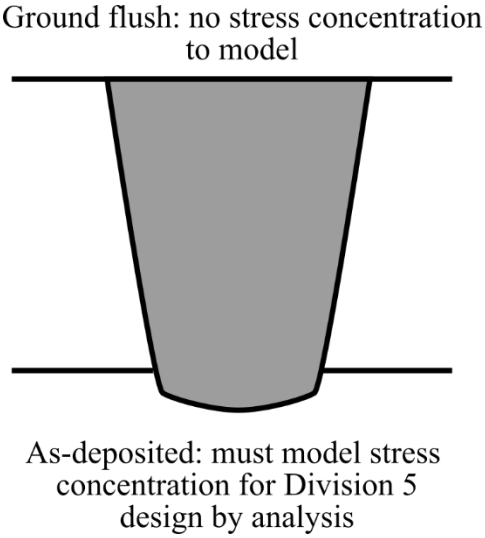

Figure 3.4. Demonstration of how for as-deposited welds the designer must include the stress concentration of the weld toe in their analysis.

In addition to the main, baseline design rules in HBB-3350 the Code also contains specific design rules for particular types of components. For the most part these are either design-by-rule exclusions from the basic, design-by-analysis approach of the general design code or additional particular requirements for certain types of welds. For example, HBB-3354 deals with welds for attached components, which references the low temperature rules in Division 1, Subsection NB. HBB-3356 contains additional rules for fillet welds, HBB-3361 contains rules for welding sections with different sizes, and HBB-3660 contains a limited set of piping-specific rules, again mostly referring to the low temperature nuclear code rules in Division 1, Subsection NB.

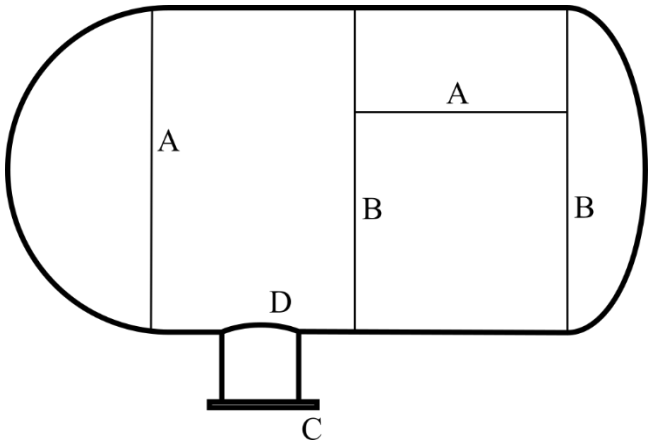

Figure 3.5. Illustration of the basic categorization of welds in a vessel. Note that the weld connecting the hemispherical head to the shell is an example of an exception from the general classification scheme: it is a circumferential joint but is category A (not category B) because it connects a hemispherical head to the vessel shell.

HBB-3351 contains a key set of categorization rules for welds. This provision divides welds in Class A components into four categories (Figures HBB-3351-1 and HBB-3352-1). Figure 3.5 is a schematic categorizing different types of welds, but in brief:

- Category A: longitudinal joints within main shells, communication chambers, transitions in diameters, or nozzles; any joint in a sphere, in a formed or flat head, or within the side plates of a flat-sided vessel; and circumferential welds connecting hemispherical heads to main shells, communication chambers, transitions in diameters, or nozzles.
- Category B: Circumferential welds in main shells, communication chambers, nozzles, or transitions in diameters including joints between the transition and the shell; circumferential welds connecting formed heats other than hemispherical main shells (Category A) to main shells, to transitions in diameter, to nozzles, or to communicating chambers.
- Category C: Welded joints connecting flanges, Van Stone laps, tube-shells, or flat heads to main shells, to formed head, to transitions in diameters, to nozzles, or to communicating chambers and any weld connecting on side plate to another side plate in a flat-sided vessel.
- Category D: joints connecting communicating chambers or nozzles to main shells, to spheres, to transition in diameter, to heads, or to flat sided vessels and joints connecting nozzles to communicating chambers.

In summary (with some exceptions, see for example the joint connecting the hemispherical head to the shell in Figure 3.5), Category A joints are longitudinal joints, Category B are circumferential joints, Category C are flange connections, and Category D are nozzle connections.

The main purpose of these Categories is to define specific construction and inspection rules for each type of joint (see the next section of this report). However, HBB-3352 provides additional design restrictions for each category. For example, HBB-3352(f) provides special rules for oblique full penetration nozzle welds.

3.2.1.2 Construction and inspection

Subsection HB, Subpart B is both a design and construction code. HBB-5000 provides construction and initial inspection rules for Class A components, including welded construction. As with most of the construction and inspection rules in HBB, the particular rules in Section III, Division 5 extend the low temperature rules in Division 1, Subpart NB.

Of primary interest in HBB-5200 are the inspection rules for the different categories of welded joints described above. HBB-5210 through HBB-5240 provides rules for each category of welds. In summary these rules are:

- Category A (HBB-5210): Double volumetric inspection is required by:
  - Radiography and ultrasound
  - Radiography and eddy current
  - Two angles of radiography

  Additionally, external and accessible internal edges require ½ inch surface examination by magnetic particle or dye penetrant inspection.
- Category B (HBB-5220): For diameters greater than 4 inches, the requirements of Category A apply. For diameters less than 4 inches single volume radiography may be used, in addition to the Category A edge inspection requirements.
- Category C (HBB-5230): For diameters greater than 4 inches the Category A rules apply. For diameters less than 4 inches single volume radiography may be used, in addition to the Category A edge inspection requirements. There are special rules for Category C corner welds.
- Category D (HBB-5240): Extensive itemized requirements for particular types of Category D welds. These rules build on top of the provision of Division 1, NB-5240. Many, but not all, types of Category D welds also required double volumetric and edge inspection per the Category A criteria.

In short, the majority of welds in Class A components require a double volumetric inspection and both an inner and outer edge inspection. In addition, HBB-5130 requires dye penetrant inspection of weld preparation surfaces. The challenges associated with hot cracking, stress concentration due to the metallurgical notch effect, and the potential for microstructural changes in weldments at high temperature justify these rather stringent inspection criteria.

3.2.2 Class B components

Subsection HC, Subpart B contains rules for the design and construction of elevated temperature Class B components. These rules are generally less stringent than the Class A rules in Subsection HB, Subpart B, reflecting the lower safety consequences for Class B components.

The design rules are based on primary load and buckling checks – Class B components do not require a strain accumulation or creep-fatigue check. As with Class A components, the Code does not contain detailed buckling rules but rather provides load factors and a general requirement to assess the component for buckling.

The main design check is then a primary load limit based on an allowable stress approach with allowable stresses defined in HBC-II. The Class B allowable stresses are similar to the Design

Load allowable stress S_o from the base metal design rules (see above) in that they nominally do not depend on the design life but are based on 100,000-hour time-dependent properties. This is analogous to current Section I/Section VIII non-nuclear commercial practice. Figure HCB-II-1000-1 provides a flow chart for determining the allowable stress given the component type and the Service Level of the loading under consideration.

The default approach is to use the allowable stresses in Tables HCB-II-3000-1 to -4. The alternative approaches provide higher allowable stresses, given in Tables HBC-II-2000-1 to -4, provided certain criteria are met. Essentially, the alternative approaches are to first demonstrate that creep is negligible and then apply time-independent allowable stresses, reduced for thermal aging by factors listed in Table HCB-II-2000-5, if appropriate. Mandatory Appendix HCB-III provides the negligible creep criteria, which do not have special rules for weldments. The allowable stress tables for the negligible creep criteria do provide efficiency factors for welds less than 1.0, depending on the type of weld and the type of inspection performed. This in contrast with the HBB approach for Class A components, which assumes overmatched welds in the time-independent sense. However, it reflects the wider range of materials and welds allowed for Class B construction.

If the negligible creep criteria are not met the designer uses the allowable stresses in Tables HCB-II-3000-1 to -4. Of crucial importance for welds these allowable stresses must be multiplied by the appropriate weld reduction factor from Tables HCB-II-3000-5 to HCB-II-3000-9. *Welds not listed in these tables (i.e. welds without defined weld reduction factors) are not allowed for use in Class B construction in the non-negligible creep regime.* This is a critical gap in the current Code rules, discussed in detail in Section 3.3 below.

The inspection requirements for Class B components are those of Division 1, Article NC-5000 covering low temperature Class II components. The high temperature Code provides some supplemental construction rules for fillet welds listed in HCB-4427.

3.2.3 Core support (HGB)

Subsection HG, Subpart B provides rules for the design and construction of metallic core support components (Class SM) operating in elevated temperature conditions. These are often safety-critical but unpressurized components. The design and construction rules are extensively based on the HBB rules for the design and construction of Class A components. In fact, the majority of HGB is a word-for-word duplication of HBB. As such, this report does not contain an additional summary of the weld rules for HGB. For details of the weld design and construction rules for Class SM components see Section 3.2.1 above.

3.3 Time-temperature gaps

This section addresses time-temperature gaps in the weld design and construction rules described above. Specifically, this section identifies weld types (combinations of base material, weld filler, and welding technique) that might be required in the construction of new high temperature reactors but are not currently supported by the ASME Code.

3.3.1 Existing allowable welds

The current Code only allows a limited number of weld types in Class A construction, as described by Tables HBB-I-14.10A-1 to HBB-I-14.10E-1. The weld stress rupture factors are given (generally) as a function of temperature and time. However, the current tables of rupture factors are not comprehensive – there are combinations of temperature/time that are permissible for base material construction but where the current Code does not provide stress rupture factors for certain types of weldments (and hence, they are not approved for use)

Table 3.1 summarizes these gaps. The table lists the base material, weldment type, and the corresponding time-temperature ranges allowed for base material and welded construction. Gaps in the current rules are highlighted. Note that Alloy 617 is not yet part of the base Code, but has been approved for Class A construction through a recently approved Code Case (N-898).

Table 3.1. Summary of allowable base/weldment combinations with time/temperature gaps highlighted.

Base material	Max time (hours)	Max temperature (°C)	Weldment	Max time (hours)	Max temperature (°C)
304H	300,000	800	SFA-5.22 E 308T and E 308LT, SFA-5.4 E 308 and E 308L, and SFA-5.9 ER308 and ER 308L	300,000	675
“	“	“	SFA-5.2 EXXXT-G, SFA-5.4 E 16-8-2, and SFA-5.9 ER	300,000	650
“	“	“	SFA-5.22 E 316T and E 316LT-2, -3, and -3, SFA-5.4 E 316 and E 316L, and SFA-5.9 ER 316 and ER 316L	300,000	750
316H	300,000	800	SFA-5.22 E 308T and E 308LT, SFA-5.4 E 308 and E 308L, and SFA-5.9 ER 308 and ER 308L	300,000	700
“	“	“	SFA-5.22 EXXXT-G, SFA-5.4 E, and SFA-5.9 ER	300,000	650
“	“	“	SFA-5.22 E 316T and E316LT-2, -3, and -3, SFA-5.4 E 316 and E 316L, and SFA-5.9 ER 316 and ER 316L	300,000	750
Alloy 800H	500,000	900	SFA-5.11 ENiCrFe-2 (INCO A)	300,000	750
			SFA-5.14 ERNiCr-3 (INCO 82)	300,000	750
2.25Cr-1Mo	300,000	650	SFA-5.28 E 90C-B3, SFA-5.28 ER 90S-B3, SFA-5.5 E 90XX-B3, SFA-5.23 EB 3, SFA-5.23 ECB 3, SFA-5.29 90T1-B3	300,000	650
Grade 91	500,000	650	SFA-5.28 ER 90S-B9, SFA-5.5 E90XX-B9, SFA-5.23 EB9	Unlimited	650
Alloy 617	100,000	950	SFA-5.14, ERNiCrCoMo-1 (GTAW only)	Unlimited	950

In summary, there are temperature gaps for 304H and 316H – no weldment can be used in the 750 to 800° C temperature range. There is both a time and temperature gap for Alloy 800H – no weldment can be used for design lives greater than 300,000 hours nor temperatures in the 750 to 900° C range. Whether these gaps are a limitation on reactor design depends on the reactor type.

However, salt reactors using 316H stainless steel will likely require metal temperatures in excess of 650° C, meaning additional weld qualification work may be required to fulfill design needs.

While the 2019 edition of the Code does not provide Grade 91 rupture factors as a function of time, recent data suggests that time-dependent factors are required to ensure the long-term integrity of welded components [30]. While time-dependent factors have not yet been approved by the relevant code committees, a current proposal under consideration includes factors covering the entire base metal allowable temperature/time range (500,000 hours and 650° C) so that no gap is expected for this material even when the new factors are adopted.

Code Case N-898 only approves Class A Alloy 617 construction for 100,000 hour design lives. As code action increases the maximum base metal design life the weld factors will need to be similarly extended.

3.3.2 Commercial weld types not permitted by Division 5

As noted in the sections covering the design rules, non-listed welds are not allowed for use in Class A or Class B construction. That is, if the appropriate section of the Code (HBB for Class A, HCB for Class B, HGB for Class SM) does not provide weld rupture factor for the weldment then it cannot be used in the creep range. This means for Class A and SM designers are limited to the weld/base/electrode combinations listed in Table 3.1.

This list is fairly comprehensive for the Class A materials, though there may be a few gaps. For example, Alloy 617 is commonly used as an overmatched filler for weldments in 800H base metal construction. Currently this combination is not allowed by the Code. These gaps are comparatively minor, as the majority of suitable weldments used for the six Class A materials are included in the Code.

Welded Class B components operating in the non-negligible creep range present a larger gap. As noted in Section 3.2.2, only Class B components constructed using weldments with rupture factors listed in Tables HCB-II-3000-5 to HCB-II-3000-9 can be used. These tables are identical to Tables HBB-I-14.10A-E from HBB, taking values from those time-dependent tables for 100,000 hours design life. This means that currently the only materials allowed for welded Class B construction for components operating in the creep range are the five Class A materials (and associated weldments) listed in HBB: 304H, 316H, Alloy 800H, 2.25Cr-1Mo, and Grade 91. A simple Code action should be adopted to include Alloy 617 in this list when the Alloy 617 Code Case is merged into the main text of the Code (a special nuclear Code Case could be adopted instead if a vendor has a critical need for Class B Alloy 617 construction). This limitation on welded Class B construction is a critical gap in the current Code as it severely limits designer options for Class B components.

There is no simple fix to this gap in the current rules as generating an extensive database of cross-weldment creep rupture tests, required to develop rupture factors, is infeasible for the large list of Class B base materials. A feasible solution is for vendors to identify priority materials for use in their reactors for Class B components and welds could be qualified for high temperature Class B construction from this reduced list of materials. Such a project could be supported either by the vendors themselves or through a government-sponsored research program. An alternative strategy

could be to explore the use of conservative rupture factors for categories of materials, rather than the material-specific factors in the current Code.

4 Design Under Advanced SMR Specific Environments

Currently, there are more than 50 SMR designs under development for different applications around the world [31]. Almost all SMR designs adopt the concept of either the low temperature water cooled reactor or the advanced reactor. Table 4.1 provides a summary of different SMR design concepts. Based on reactor outlet temperature and coolant type the SMR designs can be categorized into – 1) Water cooled SMR, 2) Liquid metal cooled SMR, 3) Molten salt SMR, and 4) High temperature Gas cooled SMR.

Among the four categories, the liquid metal cooled, molten salt, and high temperature gas cooled SMRs are based on advanced reactor concepts and have operating temperature much higher than the water cooled SMRs. Depending on the type of environment the structural materials of advanced SMRs will experience corrosion and radiation related degradation and failure modes at elevated temperature. These degradation and failure modes could potentially reduce the strength and reliability of the structural components during service and must be accounted for to develop an adequate structural design of the advanced SMRs.

This section reviews the effect of advanced SMR environment on the degradation and failure modes of structural alloys for high temperature nuclear components. This chapter also surveys the ASME Section III, Division 5 rules for design in adverse environments and proposes several mitigation actions that can be taken to fill the gaps in the design rules.

Table 4.1. Summary of SMR designs based on core exit temperature [31].

Category	***Neutron Spectrum***	***Coolant***	***Core exit Temperature, T (°C)***
Water cooled SMR	Thermal	Light water, High purity water	T<390
Liquid metal cooled SMR	Fast	Sodium, Lead, Lead-Bismuth	400<T<565
Molten salt SMR	Thermal, Fast	Molten salt	565<T<720
High temperature gas cooled SMR	Thermal, Fast	Helium	T>720

lead or lead-bismuth can be used as a coolant for a core exit temperature up to 800°C.

4.1 Failure mechanisms under irradiation

The structural alloys of advanced SMRs are expected to exhibit several irradiation-induced degradation mechanisms such as radiation hardening and loss of ductility, irradiation creep, irradiation growth, and high temperature helium embrittlement. Fundamentals to all these irradiation-induced degradations are the basic damage production through two primary processes – the creation, diffusion, and interaction of point defects such as vacancies and interstitial atoms resulting from collisions with high energy neutrons; and the chemical and isotropic alteration of atoms via transmutations [32].

Since the rate-controlling energies for these processes are approximately proportional to the material's melting point, the transition temperature between different irradiation degradation mechanisms can be approximated by using homologous irradiation temperature (T/T_M, where T_M is the melting temperature) [33]. Figure 4.1 summarizes the approximate temperature regimes where different irradiation degradations are most pronounced in structural metallic alloys. Obviously, a precise determination of the temperature regimes also depends on several other factors such as

alloy composition, grain size, displacement dose, etc. Detailed discussion on the underlying mechanism for each damage process is beyond the scope of this report. Several chapters in [32] and in [34] provide detailed reviews of radiation-induced microstructural changes, radiation damage formation, and radiation-induced segregation in metallic alloys. This section focuses on radiation related mechanical property changes and failure modes for reactor structural metallic alloys.

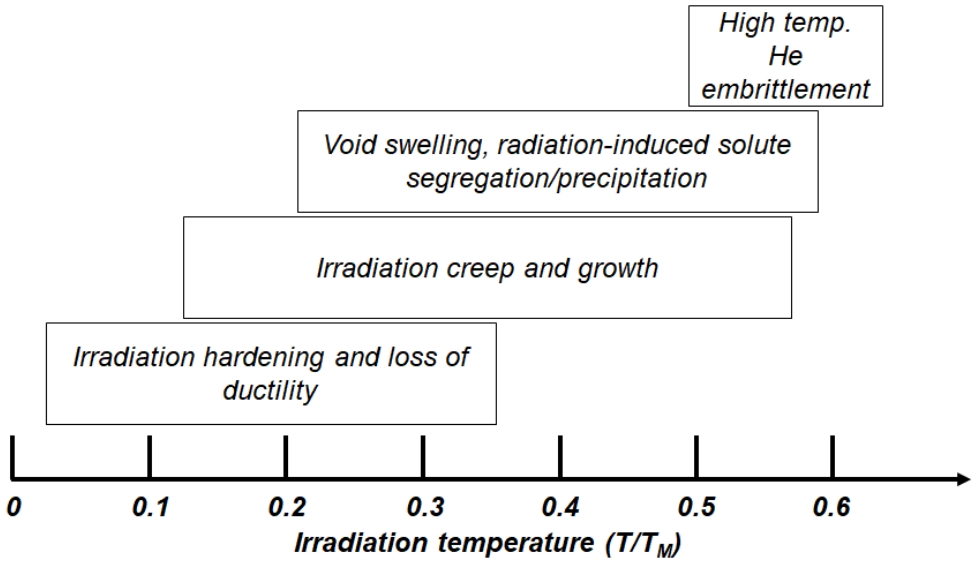

Figure 4.1. A general overview of the temperature regimes where different radiation-induced degradation mechanisms are most prominent in structural alloys [33].

4.1.1 Irradiation hardening and loss of ductility

Neutron irradiation creates fine-scale defect clusters, including dislocation loops, gas-filled bubbles, precipitates, and solute-defect clusters in structural metallic alloys [35]. These defect cluster act as obstacles to the movement of dislocations and therefore increase the strength of metal. This increase of strength is typically most pronounced below a characteristic material- and dose rate-dependent temperature. Above this characteristic temperature, the radiation hardening diminishes with increasing temperature [33] as indicated in Figure 4.2 for Alloy 617 and Alloy 800H [36].

For most materials, the irradiation hardening at a given dose is either nearly constant or decreases slowly with increasing temperature below the characteristic temperature [33]. In some materials, however, a localized peak in irradiation hardening can occur at an intermediate temperature. This is due to the processes such as irradiation-induced and -enhanced precipitation or the helium bubble formation that introduce additional obstacles to dislocation movement. An example of this phenomena is shown in Figure 4.3 for austenitic stainless steels [37].

Moreover, the radiation hardening usually saturates at a low irradiation level. This saturation level depends on metal composition and temperature and interestingly does not depend on heat treatment such as annealing, cold-work etc. For example, as shown in Figure 4.4, the yield strength of 20%

cold-worked 316 stainless steel and annealed 316 stainless steel converges to the same saturation level when irradiated under same dpa rate and temperature [38].

Although irradiation hardening, i.e. the increase in strength, is nominally beneficial when compared to the strength decrease that may occur in alloys during long-term thermal aging, the radiation hardening is typically accompanied by reductions in ductility [39]. Usually, tensile ductility increases with the decrease of irradiation hardening due to the increase in operating temperature. However, reverse trend was observed by Nanstad et al. [36] for Alloy 617 and Alloy 800H, as shown in Figure 4.5.

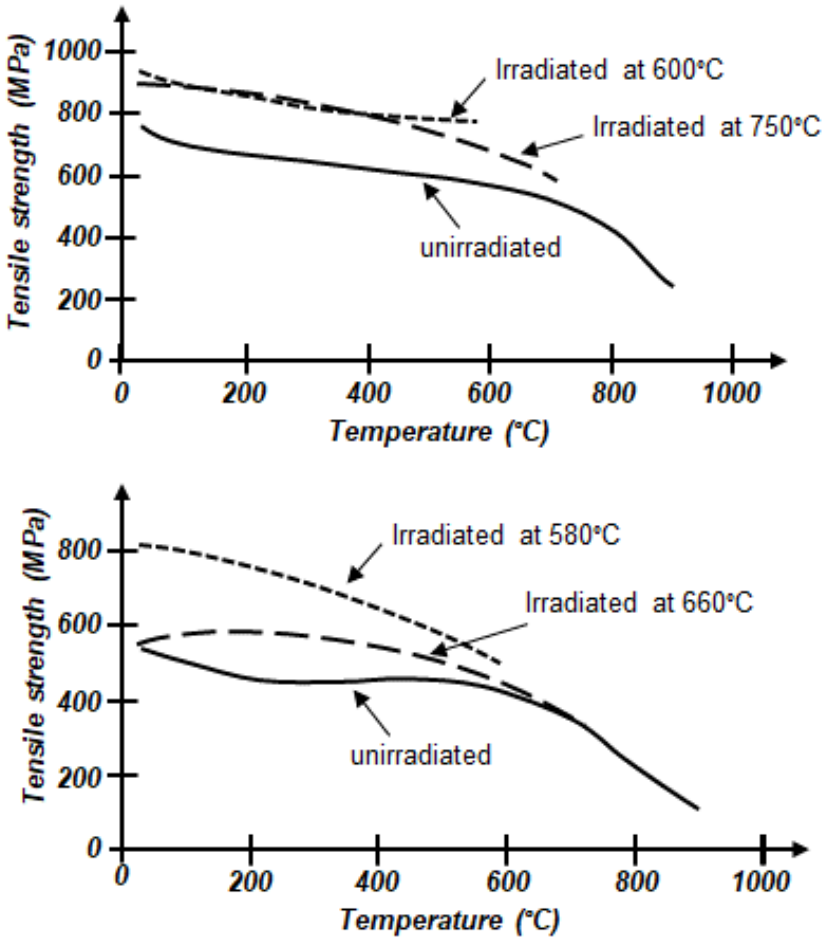

Figure 4.2. Comparison of tensile strength between unirradiated and irradiated Alloy 617 (top) and Alloy 800H (bottom). Total irradiation was about 1.42 dpa and 1.45 dpa, respectively for Alloy 617 and Alloy 800H. Trend line from [36].

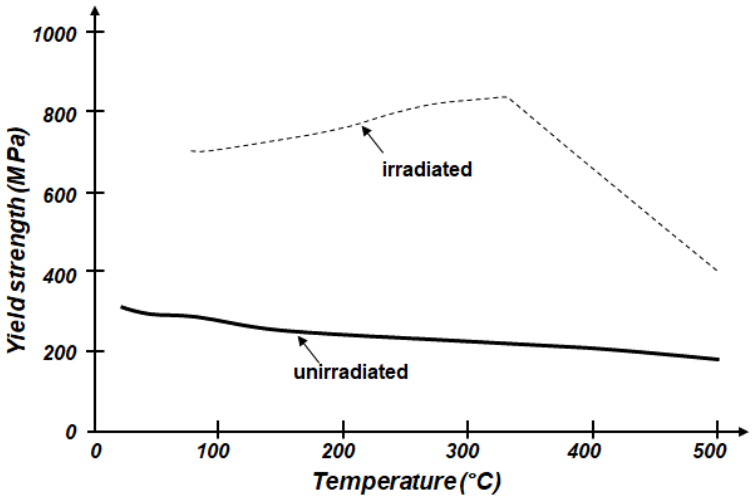

Figure 4.3. The trend in yield strength of several solution annealed type 316 and PCA austenitic stainless steels as a function of temperature. The irradiation temperature is equal to the test temperature and the neutron doses range from 3 to 20 dpa. Trend line from [37].

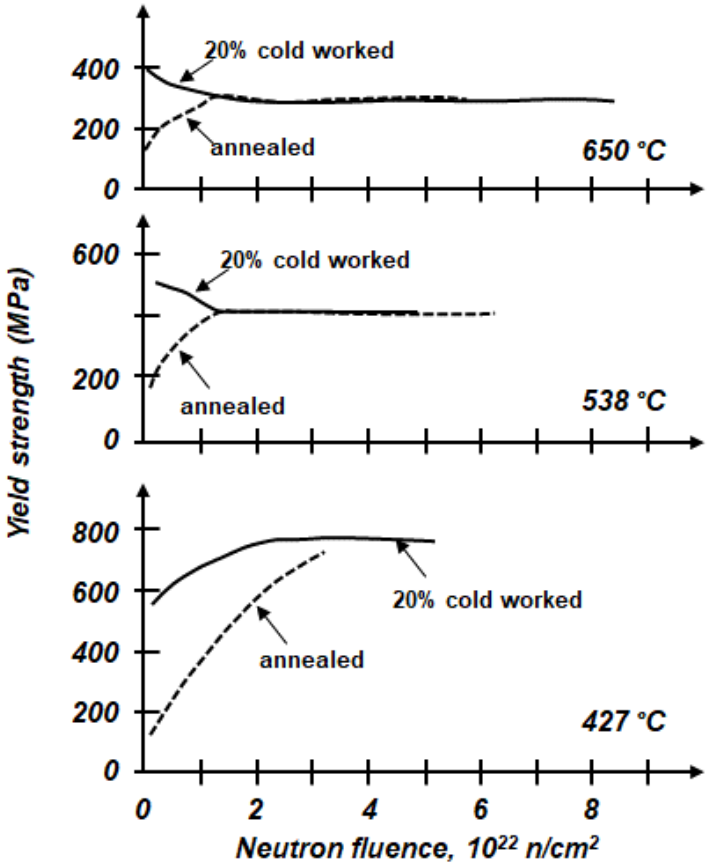

Figure 4.4. The trend in yield strength evolution as a function of temperature, neutron irradiation, and heat treatment for type 316 austenitic stainless steel. Trend line from [38].

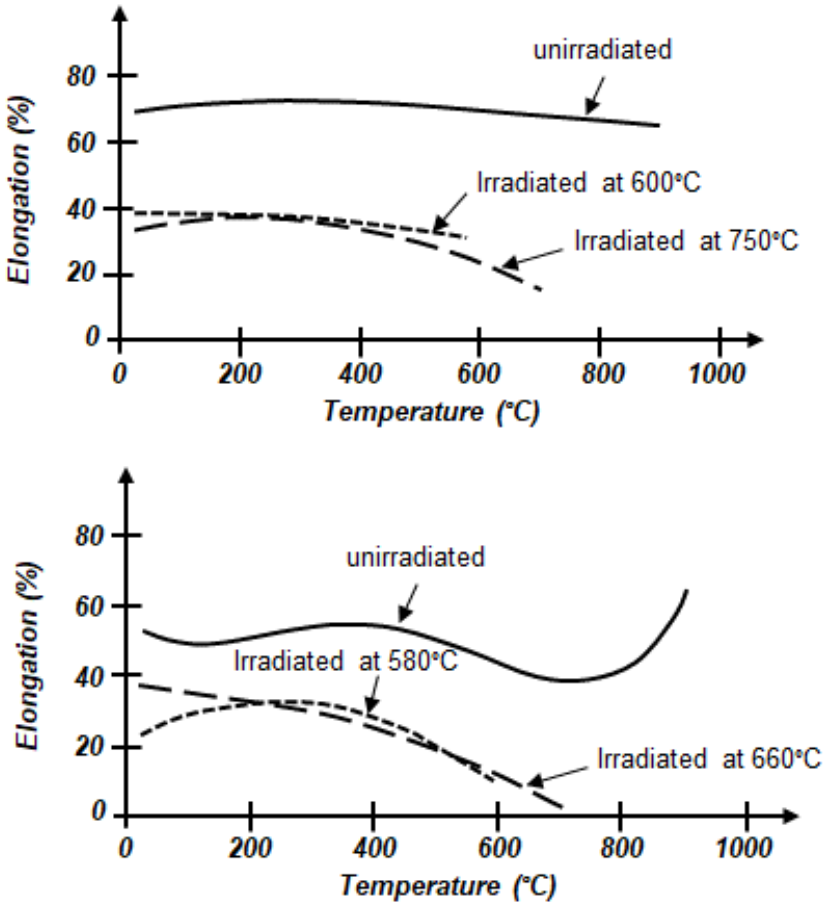

Figure 4.5. Comparison of total tensile elongation between unirradiated and irradiated Alloy 617 (top) and Alloy 800H (bottom). Total irradiation was about 1.42 dpa and 1.45 dpa, respectively for Alloy 617 and Alloy 800H. Trend line from [36].

4.1.2 Irradiation creep and growth

Irradiation creep is a stress-induced dimensional change under irradiation at intermediate temperatures. It is the response of the dislocation microstructure to the local stress state and typically most pronounced in the temperature regime ~0.2-0.45 T_M [33]. In this regime, the irradiation-induced deformation can be orders of magnitude larger than that from thermal creep. As operating temperature increases, however, the exponential increase of thermal creep deformation leads to a transition to thermal creep dominated behavior [40]. Figure 4.6 compares the conventional thermal creep deformation with the in-reactor creep deformation for austenitic steel. As indicated by the figure, the irradiation creep is characterized by a relatively weak dependence on temperature but by a progressive deformation increase with increasing the dpa level at a given temperature.

Irradiation creep is widely held to be non-damaging at the microstructural level because it does not enhance void nucleation or growth at the grain boundaries [41]. Moreover, irradiation creep can mitigate thermal creep damage by relaxing stress and allow deformation without failure. Furthermore, the plastic strain produces by irradiation creep is less than 1% under moderate operating stresses (~50-100 MPa) for doses below ~100 dpa if the void swelling is small [33]. In the 1970s, swelling and irradiation creep were used to be considered as two separate processes but now it is known that both are interrelated and interactive processes [41]. Irradiation creep can operate before

the onset of swelling but is accelerated when swelling begins. Therefore, the dimensional changes due to irradiation creep is generally only of concern for high stress and high dose conditions or cases where void swelling is significant.

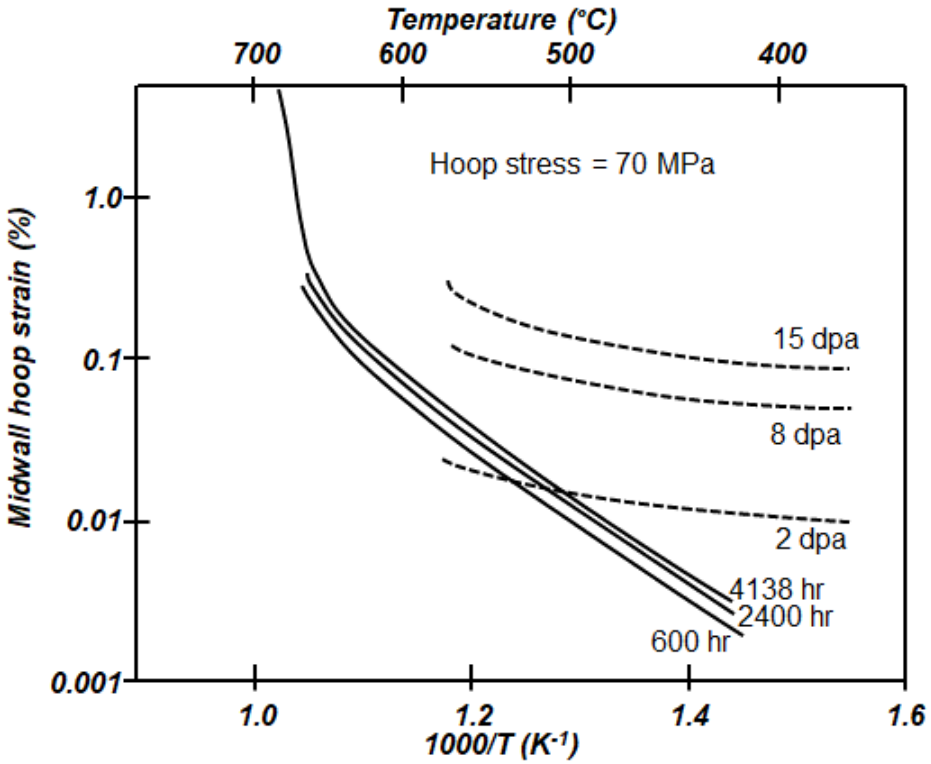

Figure 4.6. Temperature dependence of in-reactor and thermal creep for 20% cold worked Type 3 16 stainless steel. Trend line from [40].

Irradiation growth is a volume-conservative anisotropic distribution of strains without the presence of stress [42]. It is usually observed in anisotropic crystalline materials such as graphite and most prominent at low-to-intermediate irradiation temperatures [43]. Irradiation growth typically produces moderate anisotropic dimensional changes (0.1%–1%) which is generally less pronounced than irradiation creep or swelling [33]. However, engineering design should account for the dimensional changes due to the irradiation growth, particularly due to the anisotropic growth and the shrinkage aspect of the dimensional changes.

4.1.3 Void swelling

Void swelling is the progressive accumulation of vacancies that are introduced by displacement damage to concentration levels that are far beyond the thermal equilibrium. Void swelling can occur in all irradiated materials at irradiation temperature regime ~0.3-0.6 T_M [33]. Void swelling is the most heavily researched and published irradiation-induced phenomenon as it has been recognized as a potential major contributor to dimensional instability in nuclear reactor structural components. In the absence of stress field or constraint, swelling distributes its strains isotopically.

When constrained or spatially varying, however, swelling can lead to high stresses and activate irradiation creep which then redistributes the strain anisotopically [41].

Void swelling typically exhibits a transient or incubation regime where no or very low swelling occurs before swelling moves to a steady-state rate with the increase of dose. Figure 4.7 summarizes the void swelling in irradiated type 316 austenitic steel at different temperatures. As indicated by the figure, the steady-state swelling rate is relatively insensitive to the initial thermomechanical conditions or to the irradiation condition once it enters the post-transient rapid swelling regime. However, the onset of the rapid swelling, defined by the termination of the transient regime, is dependent on both irradiation temperature and dose. The duration of the low-swelling transient regime is longest at either very low or very high temperatures.

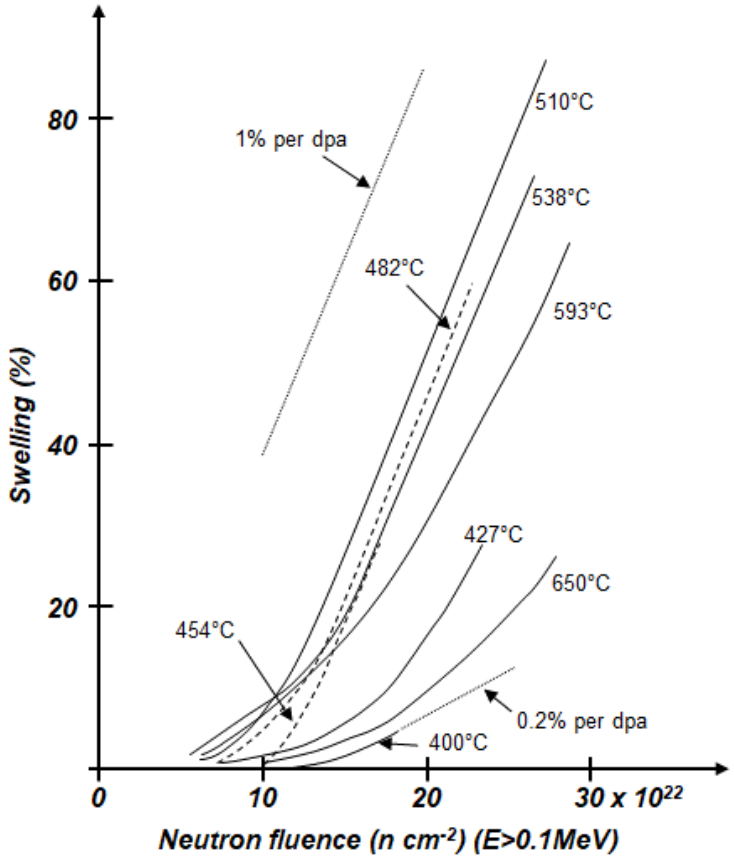

Figure 4.7. Swelling as a function of irradiation temperature and dose, as observed for 20% cold-worked type 316 austenitic steel irradiated in the EBR-II fast reactor. Trend line from [44].

Since most materials exhibit high swelling rates (0.2%-1%/dpa) in the post-transient steady state swelling regime, research on void swelling has focused on prolonging the duration of transient regime. The termination of the transient regime requires favorable conditions for both void nucleation and rapid void growth. Attaining a sufficient number of supersaturation vacancies is a key requirement for void nucleation. Since rapid diffusion at higher temperature reduces the concentration of irradiation-induced vacancies, the irradiation temperature should be low enough to

achieve a steady-state vacancy concentration well above the thermal equilibrium value [33]. Therefore, void swelling only occurs over a limited temperature range. The typical temperature range for void swell in neutron-irradiated austenitic steels and nickel-based alloys is ~350-700°C [45]. Appling some amount of cold work (20-25%) has been found to effective in suppressing void nucleation for type 316 austenitic steel [44].

In addition to sufficient vacancies, the rapid void growth requires the dislocation network to be a glissile network capable of moving mass quickly [41]. Voids embedded in a sessile microstructure are primarily composed of Frank loops and cannot grow rapidly. Therefore, significant unfaulting of Frank loops is required for the onset of high swelling rate. The unfaulting of irradiation induced Frank loops can be significantly enhanced by the applied stress.

Swelling has been observed to depend on the crystal system. As shown in Figure 4.8, 9-12 Cr ferritic/martensitic steel (bcc structure) has superior swelling resistance compared to 304 and 316 austenitic stainless steels (fcc structure) due to its longer transient regime. Lower bias towards attracting or accumulating interstitials, higher probability of vacancy recombination due to higher mobility, and a strong interaction between dislocations and interstitials are recognized as possible mechanisms for the superior swelling resistance of bcc structures [46], [47].

Swelling appears to be an unstable process for fcc metals and can be a life limiting phenomenon for reactor core components that use austenitic stainless steels, such as type 304 and 316 [48]. However, increasing the nickel content to an intermediate level, as shown in Figure 4.9, notably reduces the amount of swelling [49]. Therefore, nickel based fcc alloys such as Alloy 617 (min.

44.5% nickel) and Alloy 800H (30-35% nickel) are expected to show higher swelling resistance than type 304 (8% nickel) and type 316 (10-14% nickel) austenitic steels.

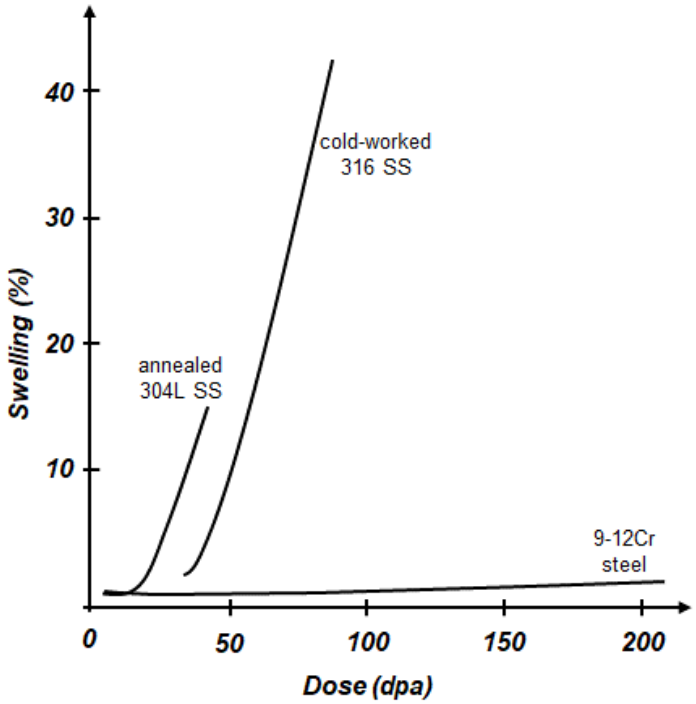

Figure 4.8. Comparison of swelling in type 304L and cold-worked 316 austenitic stainless steels and 9-12 Cr ferritic/martensitic steel, as irradiated at ~400-550°C to high doses in a fast fission spectrum. Trend line from [46].

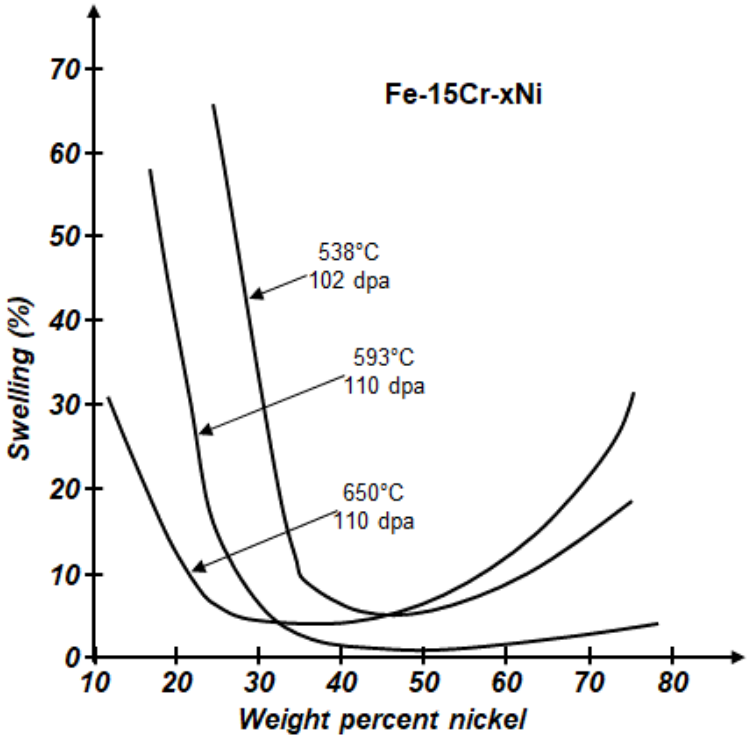

Figure 4.9. Effect of nickel content on swelling behavior of Fe-Cr-Ni alloys. Trend line from [49].

4.1.4 High temperature helium embrittlement

Under irradiation helium can be generated by transmutation reactions. Due to its very low solubility in metals, helium has a strong tendency to precipitate out into bubbles. These bubbles grow under the influence of temperature, stress, and continuous helium generation [50]. At high temperature, these bubbles can migrate to the grain boundaries and can lead to premature failure of components that are mechanically stressed. Because it is a diffusion-activated process, the helium embrittlement typically occurs at temperature above $0.5T_M$ and it becomes progressively more prominent with the increase of temperature and stress [33]. Helium embrittlement can result in dramatic reductions in ductility and therefore is an important design concern for neutron irradiated structural components at high temperatures.

Alloys with high nickel content are more susceptible to helium embrittlement due to the relatively large helium production from nickel during neutron reactions. While ferritic-martensitic steels, due to very low nickel content, exhibit superior resistance to high temperature helium embrittlement compared to austenitic steels[47], [51]. Moreover, ferritic-martensitic steels have higher size threshold for the critical radius that is required for the conversion of subcritical grain boundary bubbles to rapidly growing cavities [52]. A higher threshold means more helium is required for the bubbles to reach the critical radius.

4.1.5 Effect of irradiation on creep-fatigue failure

Irradiation induced degradation can influence the creep and fatigue behavior of materials. Although very few studies are found in literature that focus on creep-fatigue interaction under irradiation, significant amount of work has been done on investigating the effect of irradiation on creep

rupture and fatigue life. The below reviews literature on irradiation effect on creep and fatigue damages separately first before reviewing the effect on combined creep-fatigue damage.

Grossbeck et al. [53] investigated the effect of irradiation on creep rupture life of austenitic stainless steels. They found significant reduction in lives for specimen irradiated in the BR-2, a mixed-spectrum research reactor in Belgium, at 700°C. They attributed the reduction of creep rupture life to helium bubble growth and coalescence. They also noticed a change in stress dependence of the creep-rupture strength at higher stress. This can be better explained by comparing the creep rupture life of in-reactor and post-irradiation specimens, as discussed below.

Several studies [54], [55] reported lower creep rupture life for in-reactor specimens when compared to specimens tested after irradiation even though the post-irradiation specimens have higher helium concentration. The presence of tensile stress during irradiation enhances the growth of bubbles, some of which might grow as voids by vacancy absorption, cause the specimen to fail earlier than the post-irradiated samples. For example, the creep rupture life of 316 stainless steel was about a factor of 10 lower in specimens where helium was introduced continuously during the creep tests at 750°C under an applied stress in 50–110 MPa range compared to specimens that were helium hot-preimplanted with zero stress prior to creep tests [56].

The effect of irradiation on 20% cold-worked type 316 stainless steel was evaluated by Ukai et al. [57] through comparing in-reactor creep rupture tests with creep rupture experiments in air and sodium. They observed shorter creep rupture life for in-reactor specimens than those tested in air and sodium. Interestingly, however, the in-reactor creep appeared to show earlier onset of tertiary stage and was significantly accelerated. The observed higher creep strain does not support the failure mechanism associated with helium embrittlement. It was instead attributed to the earlier recovery of dislocation structure introduced by cold-working. Irradiation was also found to adversely affect the creep rupture properties of nickel-based alloys and ferritic-martensitic steels in several studies [58]–[61].

Typically, the fatigue life of nuclear metal alloys such as austenitic steels, ferritic-martensitic steels, and nickel-based alloys is reduced due to the irradiation-induced defect clusters. However, the extend of the effect can vary significantly depending on the composition, irradiation conditions, and temperature. Kharitonov [62] reviewed the low cycle fatigue data up to 1984 and provided a comprehensive review of the effect of irradiation on fatigue life of type 316 and type 304 austenitic stainless steel. Compared to type 304 stainless steel the fatigue life of 316 stainless steel was found to be strongly affected by irradiation. The life of 304 stainless steel was decreased by a factor of 1.5 to 2.5 with increasing temperature whereas that was decrease by a factor of 2.5 to 10 for 316 stainless steel. The greater reduction of fatigue life for 316 stainless steel is attributed to the higher concentration of gaseous products, especially helium and hydrogen, from transmutation of 316 stainless steel than 304 stainless steel. The main contribution of these gases comes from nickel whose content in 316 stainless steel is 13.6%, higher than 9.5% nickel in 304 stainless steel. Similarly, the decrease in fatigue life of Alloy 800H by a factor of 5 to 35 was attributed to its high nickel content of 32% [62].

Irradiation hardening was also found to affect the fatigue life of structural alloys. Fatigue life of solution annealed 316L stainless steel, as reported in [63], was not reduced by irradiation when

the applied strain was low. Due to irradiation hardening the deformation may become almost entirely elastic at low strain range which may result in a delayed crack initiation.

Most of the studies found in literature performed fatigue tests on post-irradiated specimens to determine the effect of irradiation on the fatigue life of structural alloys. However, this may not be the actual representation of the material behavior under irradiation. For example, as shown in [64] for ferritic-martensitic steel, the fatigue lives of specimens tested under irradiation were found shorter than the post-irradiated sample, while the opposite was observed in [65]. Simultaneous irradiation and fatigue can develop a different microstructure and lead to different material response which are not considered in post-irradiation experiments.

A very limited number of studies investigated the effect of irradiation on creep-fatigue behavior of structural alloys. Scholz et al. [66], [67] performed fatigue and creep-fatigue experiments on cold worked and anneal 316L stainless steel under deuteron irradiation. They conducted all the tests on hour glass specimens in torsion mode. While they compared fatigue life of irradiated specimens with unirradiated specimens, they did not compare the creep-fatigue life between irradiated and unirradiated conditions and therefore the effect of irradiation on creep-fatigue life cannot be determined. Brinkman and coworkers [68], [69] investigated creep-fatigue interaction in irradiated and unirradiated solution annealed type 316 and type 304 stainless steels based on the available data in literature. They found significant reduction in creep-fatigue life under irradiation but did not make any recommendation on estimating creep-fatigue damage under irradiation due to the lack of data.

4.2 Failure mechanisms in corrosive environment

4.2.1 Liquid metal

Liquid sodium and liquid lead and lead-alloys have been considered as coolants for fast spectrum nuclear systems. Liquid sodium was a typical choice due to its low melting point, excellent heat transfer properties, and neutron transparency [70], [71]. However, it is also operationally challenging due to high chemical activity with water, water vapor, and air, making prevention of leaks of sodium an important challenge. The low boiling point of sodium also raises the safety concerns regarding unprotected transients leading to a coolant heat up. The choice of liquid lead and lead-bismuth eutectic alloys was motivated by their high boiling point and compatibility with air, water, and steam, thereby no need for intermediate coolant loop [71]. Exposure to both types of coolant can affect the mechanical performance of reactor structural materials.

Natesan et al. [72] summarized the influence of sodium exposure on mechanical properties including tensile, creep, fatigue, and creep-fatigue of several reactor metallic alloys. They evaluated the effect of sodium exposure by comparing the mechanical properties data in air and sodium. Carburization and decarburization were found to be the key factors determining the tensile and creep properties of the alloys. The overall impact of sodium exposure (up to 5000 hr) over the temperature range 400°C ~ 800°C on tensile properties of Type 316 austenitic steel was found to be insignificant though a slight increase in tensile strength and a slight decrease in ductility due to carburization (resulting from sodium exposure) were observed in few specimens. Decarburization of 2.25Cr-1Mo steel in sodium environment at temperatures up to 550°C progressively reduces the tensile and yield strength of the steel. Similarly, loss of creep rupture strength due to decarburization was observed for 2.25Cr-1Mo. The creep rupture properties of Type 316 stainless steel were

found to be little changed after exposure in sodium for 10,000 hr at 593°C. A beneficial effect of sodium exposure on fatigue life was observed for both austenitic Type 316 stainless steels and 2.25Cr-1Mo ferritic-martensitic steels. However, the beneficial effect vanished when a tensile hold time was applied.

Kannan et al. [73] investigated the fatigue and creep-fatigue behavior of modified 9Cr-1Mo ferritic-martensitic steel (Grade 91) in sodium environment at 550°C and 600°C. Both the fatigue and creep-fatigue lives were found to be increased significantly in flowing sodium environment compared to in-air test results. Their test data are tabulated in Table 4.2.

Table 4.2. Effect of sodium exposure on fatigue and creep-fatigue life of modified 9Cr-1Mo steel [45].

Temperature (°C)	Hold time (min)	Cycles to failure	
		air	Sodium
873	0	477	2290
	1 (tensile hold)	360	1550
	1 (compressive hold)	328	2675
	10 (tensile hold)	349	582
823	0	575	2100
	10 (tensile hold)	-	1180

While much work has been done to understand the effect of sodium exposure on mechanical properties of reactor structural materials, the understanding is less advanced for exposure in lead and lead alloys [70]. Gorse et al. [74] summarizes the influence of liquid lead and lead-bismuth eutectic on tensile, fatigue, and creep properties of Type 316 austenitic stainless steel and T91 ferritic-martensitic steel, obtained in different organizations participating to the EUROTRANS-DEMETRA project. Tensile properties of both Type 316 stainless steel and T91 steel were found to be unaffected in lead and lead-bismuth. However, some ductility was lost when the steels are exposed to lead-bismuth under reducing conditions (lead-bismuth eutectic was made reducing by adding pure Mg). Only a weak damaging effect of lead and lead-bismuth was found in fatigue properties of Type 316 stainless steel. However, T91 showed a significant decrease in fatigue strength when exposed to lead and lead-bismuth which was further amplified under reducing conditions. Creep-rupture tests of T91 in flowing lead-bismuth showed a significant reduction of the time to rupture, a higher strain in primary creep phase, an earlier onset of tertiary creep. These lead-bismuth assisted creep effects amplified with increasing the stress level, notably above 180 MPa. The effect of lead and lead bismuth on creep properties of austenitic steel was not discussed.

4.2.2 Molten salts

Molten fluoride and chloride salts offer attractive characteristics – such as high volumetric heat capacities and high boiling point – to be used as coolants for nuclear reactor [75]. However, they are highly corrosive for many structural alloys, especially alloys with high chromium content which are subject to depletion of chromium into the salt [70]. Unlike in oxygen environment, the corrosion protective chromium oxide layer does not form in molten salt environments. Besides the material loss the molten salt environment can also affect the mechanical performance of metallic

materials. However, there is a paucity of literature on the mechanical properties of structural alloys in molten salt environments, except for creep.

The high temperature corrosion-creep interaction was investigated in [76]–[82] for different metal-salt systems, simulating the aircraft, marine, and land-based gas turbine engines. Most of these studies did not find significant effect of molten salt on the secondary or minimum creep rate. However, the tertiary region of creep was adversely affected by molten salt and resulted in consequent reduction in creep rupture life. Molten salt penetrates along the grain boundaries and coalesces with creep cavities, resulting in lower creep rupture life.

4.2.3 High temperature helium

Helium will be used as a coolant for high temperature gas cooled reactors. The gaseous helium by itself is inert and expected to have little impact on the corrosion and the structural integrity of reactor metallic components [83], [84]. However, the helium coolant is expected to contain small amount of impurities typically CO, CH_4, H_2O, and H_2, arising mainly from reactions between the pollutants – outgassing, air ingress, water/oil leaks etc. – and the hot graphite core [70], [83]–[85]. These impurities cannot be completely removed by the purification methods currently available [86]. Several studies [86]–[89] have shown that these impurities can significantly corrode the metallic materials at high temperature.

Depending on the temperature, oxygen potential, and carbon activity in the gas phase, the corrosion of reactor structural materials may involve oxidation, carburization, and/or decarburization. These processes can significantly affect the mechanical properties of reactor structural materials. Oxidation may reduce the load bearing cross-section of the reactor structural components. Moreover, internal oxide precipitates can also act as the preferential crack initiation sites [90] which may reduce the creep and fatigue resistance of the alloys. The dissolution of carbide due to decarburization can have damaging effect on the structural performance of metallic materials [91].

Huchtemann [61] performed creep rupture tests on Alloy 617 in air and in impure helium environments at 950°C. Strong internal oxidation and decarburization was observed in impure helium environments which led to reduction in creep strength of Alloy 617. Several other studies reported significant reduction in creep-rupture ductility of Alloy 617 [83], [92], Alloy 800H [84] in a carburizing environment compare to pure helium and air environments, however no significant change or an increase was observed in creep-rupture life.

Tsuji and Kondo [93] compared the low cycle fatigue behavior of several nickel-based alloys at 900°C in simulated high temperature gas cooled reactor environments with that in high vacuums. The alloys with relatively high ductility showed considerable resistance to fatigue damage while alloys with high creep strength suffered from the adverse effects of the impure helium. The observed behavior of the materials with unsatisfactory resistance in impure helium environment was attributed to their limited ductility and the susceptibility to intergranular oxidation. Although carburization may have played a role in the acceleration of fatigue damage.

Rao et al. [94] performed fatigue and creep-fatigue experiments on Alloy 617 in impure helium at 0.6% strain range. Their experimental data are compared with in-air test data from [95], as shown in Figure 4.10. As indicated by the figure the fatigue life of Alloy 617 is higher in helium than air. However, with increasing hold time in the creep-fatigue tests the cycles to failure of specimens in

helium reduces drastically and fails earlier than the in-air specimens. This indicates long exposure to impure helium environment has adverse effect on the creep-fatigue of Alloy 617.

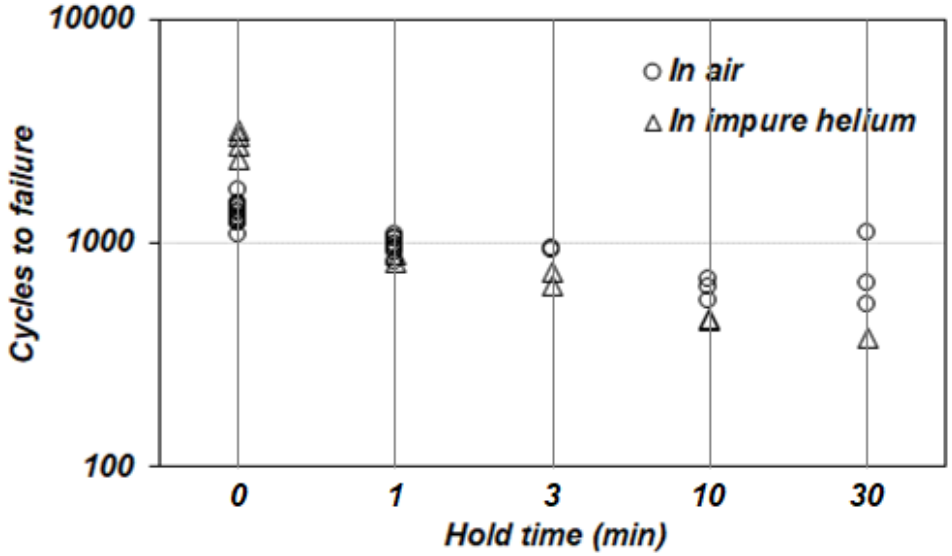

Figure 4.10. Comparison between fatigue and creep-fatigue lives of Alloy 617 in air and impure helium environments at 950°C. The applied strain range was 0.6% and all the hold times were applied in tension. The in-air data were taken from [95] *and the in-impure helium from* [94].

4.3 Gaps in ASME Section III, Division 5 rules and potential mitigation actions

The ASME Section III, Division 5 design rules for constructing high temperature nuclear reactor components do not contain any assessment rules for material degradation under irradiation and corrosion. The only explicit mention of irradiation effect on material properties is in HBB-3124. HBB-3124 cautions the designer about the increase of the ductile-to-brittle transition temperature and deterioration of fracture resistance under neutron irradiation and suggests not placing any structural discontinuities in high radiation areas. The only explicit consideration of corrosion is in HBB-3121 which requires a corrosion allowance in design thickness to account for the expected gross loss of material over the design service life under expected operating condition.

In HBB-Y-4200 the Code explicitly places the environmental degradation issues (with the exception of the effect of thermal aging on yield and ultimate tensile strength) outside the ASME code but requires the Owner/Operator to account for these issues in some way and justify their decisions to the regulator. This provision also refers to Nonmandatory Appendix W to Section III, which provides general design and construction guidance to mitigate the environmental effects. However, most of the mechanisms in Appendix W are related to low temperature light water reactors except a brief section (W-4400) covering high temperature service. Overall, although the appendix provides useful guidance, it does not provide design or fitness-for-service methods accounting for irradiation and corrosion related damage.

One straightforward approach to fill the gaps in current design method could be altering the design data to account for environmental effects relevant to advanced SMRs while keeping the overall design method to the same. These design data may include material's rupture life, fatigue life, and/or creep-fatigue interaction. A general method could be developed for specifying what experimental data is required to establish these design data for different combination of radiation dose

and coolant exposure. There may even be enough literature data for developing preliminary rupture and fatigue design data for Class A materials accounting for irradiation effects over the range of doses expected in advanced SMRs. The requirements of creep-fatigue testing to develop the interaction diagram and long-term creep testing under irradiation could be avoided by introducing adequately conservative design factors. For example, the French RCC-MRx Code uses similar conservative approach for austenitic stainless steel by applying a factor of 10 to the creep damage in non-negligible radiation environment.

Another approach for managing the effect of irradiation and corrosion on structural components could be the use of cladded components. The idea is that the Class A base material will carry the structural load while a thin clad material, joined to the base material, will serve to protect the base material from corrosion and irradiation. Use of cladded components is a well-established practice in petrochemical industry. Cladded vessels are also used in low temperature Light Water Reactors (LWRs) – typically stainless steel cladding on low alloy steel. However, design rules for cladded components are limited and to our knowledge there are currently no ASME design rules for evaluating the integrity of a clad/base system under high temperature cyclic load. The authors and others [96]–[99] have made significant progress on developing such design rules for two types of clad materials that are either much more compliant than the base metal (e.g. pure nickel on stainless steel) or much stiffer than the base metal (e.g. tungsten on stainless steel). However, reactor designers may use combinations of materials that do not fall into either of these categories if design rules are developed for such clad materials. Another issue in designing cladded components is the assessment of clad/base interface integrity under high temperature cyclic load. Reference [100] provides the details of a standardized test procedure to assess the bonding integrity of the clad/base interface under cyclic load.

A third approach could be the development of an in-situ surveillance program. The idea is to insert surveillance specimens at critical locations inside the reactor so that they experience the actual plant environmental conditions such as temperature and pressure history, exposure to coolant, irradiation, etc. The surveillance specimens would most likely to be passive, i.e., not requiring any control or loading mechanisms penetrating the primary coolant boundary, to avoid complication in the design of components. A possible design for a passively loaded specimen is a bimetallic specimen, utilizing the CTE mismatch between two materials to apply the mechanical load. Reference [101] provides the preliminary analysis results demonstrating the viability of such concept. However, the reference also discusses several issues that need to be resolved before translating the concept into a complete method for sizing specimens to replicate a set mechanical load, given some temperature history. Once the method is developed, the surveillance specimens could be designed as “canaries” [101]. That is, the specimens could be designed such that their failure before a predetermined length of time would indicate a problem with the structural design. A method could also be developed to predict the remaining life of the component via some out-of-reactor tests of the surveillance specimens.

5 Conclusions and Summary

5.1 Summary

This report summarizes the ASME Boiler & Pressure Vessel Code Section III, Division 5 rules covering the design and construction of high temperature nuclear reactor components. The focus of this summary is on the relevance of the rules to SMRs and in identifying any gaps in the rules, considering their potential future application to SMR design. The report considered base material design, weld degradation mechanisms and weldment design, and environmental effects. One chapter is devoted to each topic, and each chapter includes a summary of the key structural degradation and failure mechanisms, a survey of the ASME design rules, and a gap analysis focusing on SMRs. The report, as a whole, summarizes the application of the ASME design rules to SMRs and identifies the limitations of the ASME design and construction approach.

5.2 Key recommendations

The following list summarizes the key gaps and corresponding recommendations identified in the report. The list separates the recommendations by topic. For additional details refer to the corresponding chapter in the main body of the report.

5.2.1 Base metal/general design rules

- The report identifies specific time-temperature gaps in the design properties for the six currently-qualified Class A materials. Tables 2.14-2.16 summarize these gaps. In some cases, additional testing may be required to extend the material properties to longer times and/or higher temperatures.
- The USNRC is in the process of reviewing and potentially endorsing the rules of ASME Section III, Division 5, 2017 edition. This review process identified a set of material-specific restrictions on the currently-qualified materials, described in Table 2.17. These restrictions are not part of the Code rules, but may be mandated by the USNRC as a condition of their endorsement of the ASME design approach.
- The simplified design-by-elastic analysis rules for evaluating the Section III, Division 5 creep-fatigue and deformation limits criteria may have reduced accuracy in the temperature range where creep and plasticity become indistinguishable. Table 2.7 provides temperature guidelines for delineating this viscoplastic regime.
- The current edition of the Code (2019, continuing to 2021) does not provide reference inelastic constitutive models for use with the design by inelastic analysis method for evaluating the creep-fatigue and deformation limits. ASME is in the process of developing suitable models, starting with Grade 91, 316H, and Alloy 617.
- The list of currently-qualified Class A and Class B materials may not be optimal for some SMR concepts. This is not strictly a gap, as the ASME process generally assumes that plant designers or owners will drive the material qualification process by identifying a need

for a new material and sponsoring or driving the required material test program. However, qualifying high temperature materials requires at least some relatively long-term testing, depending on the desired component design life, and so developers and regulators should be aware of the required lead time.

5.2.2 Weldments

- There are specific time/temperature gaps in the allowable combinations of weldment type/base material identified in Table 3.1. Some of these gaps may be significant, depending on the SMR operating temperature range. These gaps could be addressed with some additional cross-weld creep testing.
- There are very few qualified Class B weldments for components operating at elevated temperatures. For welded Class B construction in the elevated temperature regime designers are essentially limited to the Class A materials. There is no easy way to address this gap, which may require cross-weld test programs for the highest priority materials or considering new Class B design methods.

5.2.3 Environmental effects

- With a few exceptions, primarily for gross section loss caused by corrosion, the ASME rules do not cover environmental effects. Structural materials in future SMRs will likely be vulnerable to environmental degradation in important material properties caused by irradiation and interaction with corrosive coolants. Reactor developers will need to mitigate or prevent these degradation mechanisms. Their strategy will depend on the type of reactor, but may include:
    - Limiting the radiation dose experienced by structural components. Limiting the exposure of key components to corrosive coolants.
    - Cladding structural components with some non-structural, corrosion- or irradiation-resistant materials. The report summarizes recent work on design rules for cladded Class A components, but these rules are not yet incorporated into the Code.
    - Dedicated in-situ surveillance programs aimed at quantifying or bounding the negative effects of radiation damage or coolant exposure. The report describes preliminary efforts to develop suitable passively actuated surveillance samples and develop a strategy for a surveillance program.
    - Accounting for the degradation in material properties caused by radiation and corrosion in the component design. The report cites the French RCC-MRx design code as an example of this approach. However, the French code focuses on one type of coolant (sodium) and there may not be sufficient data to develop a design method for the wide range of materials/coolants/radiation doses proposed by SMR developers.
- There is comparatively little data on the effect of irradiation on the creep-fatigue life of common reactor structural materials. Most past studies focus on either fatigue or creep, not the combination of both. A testing program may be needed to address this gap.

- Additional testing is needed to assess the effect of coolant exposure on mechanical properties for molten lead and molten salt coolants.

Acknowledgements

The research was sponsored by the U.S. Department of Energy, under Contract No. DEAC02-06CH11357 with Argonne National Laboratory, managed and operated by UChicago Argonne LLC. Funding and sponsorship were provided by the Canadian Nuclear Safety Commission.

References

[1] R. D. Porco, “Letter from ASME to the NRC.” NRC Accession No. ML18184A065, 2018.

[2] B. E. Thomas, “NRC response to the ASME.” NRC Accession No. ML18211A571, 2018.

[3] M. C. Messner, R. I. Jetter, and T.-L. Sham, “Establishing Temperature Upper Limits for the ASME Section III, Division 5 Design by Elastic Analysis Methods,” in *ASME 2018 Pressure Vessels and Piping Conference*, 2018, pp. PVP2018-84105.

[4] M. C. Messner, V.-T. Phan, and T.-L. Sham, “A Unified Inelastic Constitutive Model for the Average Engineering Response of Grade 91 Steel,” in *Proceedings of the 2018 ASME Pressure Vessels and Piping Conference*, 2018, pp. PVP2018-84104.

[5] V.-T. Phan, M. C. Messner, and T.-L. Sham, “A unified engineering inelastic model for 316H stainless steel,” in *Proceedings of the 2019 ASME Pressure Vessels and Piping Conference*, 2019, pp. PVP2019-93641.

[6] A. K. Dhalla, “Recommended practices in elevated temperature design: a compendium of breeder reactor experiences (1970-1987): Volume III - Inelastic analysis,” 1991.

[7] T.-L. Sham, “Historical Context and Perspective on Allowable Stresses and Design Parameters in ASME Section III, Division 5, Subsection HB, Subpart B,” 2021.

[8] R. G. Gilliland, “The Behavior of Welded Joints in Stainless and Alloy Steels at Elevated Temperatures,” 1972.

[9] J. Shingledecker, B. Dogan, J. Foulds, R. Swindeman, D. Marriott, and P. Carter, “Development of Weld Strength Reduction Factors and Weld Joint Influence Factors for Service in the Creep Regime and Application to ASME Codes,” 2017.

[10] P. Chellapandi and S. C. Chetal, “Influence of mis-match of weld and base material creep properties on elevated temperature design of pressure vessels and piping,” *Nucl. Eng. Des.*, vol. 195, no. 2, pp. 189–196, 2000.

[11] S. T. Tu, P. Segle, and J. M. Gong, “Creep damage and fracture of weldments at high temperature,” *Int. J. Press. Vessel. Pip.*, vol. 81, no. 2, pp. 199–209, 2004.

[12] J. Storesund and S. T. Tu, “Geometrical effect on creep in cross weld specimens,” *Int. J. Press. Vessel. Pip.*, vol. 62, no. 2, pp. 179–193, 1995.

[13] S. Spigarelli and E. Quadrini, “Analysis of the creep behaviour of modified P91 (9Cr-1Mo-NbV) welds,” *Mater. Des.*, vol. 23, no. 6, pp. 547–552, 2002.

[14] and T H Hyde W Sun, “Determination of Creep Proprties for P91 Weldment Materials At 625 C,” pp. 1–13.

[15] D. J. Smith, N. S. Walker, and S. T. Kimmins, “Type IV creep cavity accumulation and failure in steel welds,” *Int. J. Press. Vessel. Pip.*, vol. 80, no. 9, pp. 617–627, 2003.

[16] D. J. Abson and J. S. Rothwell, “Review of type IV cracking of weldments in 9- 12%Cr creep strength enhanced ferritic steels,” *Int. Mater. Rev.*, vol. 58, no. 8, pp. 437–473, 2013.

[17] J. A. Francis, W. Mazur, and H. K. D. H. Bhadeshia, “Type IV cracking in ferritic power plant steels,” *Mater. Sci. Technol.*, vol. 22, no. 12, pp. 1387–1395, 2006.

[18] A. Dhooge and A. Vinckier, “Reheat cracking-A review of recent studies,” *Int. J. Press. Vessel. Pip.*, vol. 27, no. 4, pp. 239–269, 1987.

[19] A. Vinckier and A. Dhooge, “Problem of Reheat Cracking in Welded Structures During Stress-Relief Heat Treatments.,” *J. Heat Treat.*, vol. 1, no. 1, 1979.

[20] M. T. Cabrillat, P. Allegre, E. Pluyette, and B. Michel, “Intergranular reheat cracking in 304H components . Experiments and damage evaluation,” in *Transactions of the 16th International Conference on Structural Mechanics in Reactor Technology*, 2001, no. August.

[21] L. Allais, Q. Auzoux, M. Reytier, and A. Pineau, “Reheat cracking in austenitic stainless steels,” in *European Conference on Fracture (ECF)*, 2002, pp. 45-14–22.

[22] S. P. Ghiya, D. V Bhatt, and R. V Rao, “Stress Relief Cracking in Advanced Steel Material - Overview,” in *Proceedings of the World Congress on Engineering*, 2009, vol. II, pp. 1737–1740.

[23] A. Gotoh, “Reheat cracking - the mechanism and countermeasures,” *Weld. Int.*, vol. 7, no. 4, pp. 266–268, 1993.

[24] ASTM International, “Standard test methods for conducting creep , creep-rupture , and stress-rupture tests of metallic materials (E139).” pp. 1–14, 2014.

[25] R. L. Klueh and J. F. King, “Elevated-Temperature Tensile and Creep-Rupture Behavior of Alloy 800H/ERNiCr-3 Weld Metal/2 1/4 Cr-1 Mo Steel Dissimiliar-Metal Weldments,” 1982.

[26] M. Law and W. Payten, “Cross weld creep testing and its extrapolation to service welds,” *Int. J. Press. Vessel. Pip.*, vol. 74, no. 2, pp. 129–133, 1997.

[27] T. H. Hyde and A. Tang, “Creep analysis and life assessment using cross-weld specimens,” *Int. Mater. Rev.*, vol. 43, no. 6, pp. 221–242, 1998.

[28] F. C. Hull, “Delta Ferrite and Martensite Formation in Stainless Steels.,” *Weld. J.*, vol. 52, no. 5, 1973.

[29] G. Lothongkum, E. Viyanit, and P. Bhandhubanyong, “Study on the effects of pulsed TIG welding parameters on delta-ferrite content, shape factor and bead quality in orbital welding of AISI 316L stainless steel plate,” *J. Mater. Process. Technol.*, vol. 110, no. 2, pp. 233–238, 2001.

[30] K. Kimura and M. Yaguchi, “Re-evaluation of stress rupture factors for grade 91 weldments based on the extended database with the data collected in Japan,” *Am. Soc. Mech. Eng. Press. Vessel. Pip. Div. PVP*, vol. 6B-2019, pp. 1–8, 2019.

[31] International Atomic Energy Agency, “Advances in Small Modular Reactor Technology Developments,” p. 150, 2014.

[32] R. J. M. Konings, *Comprehensive Nuclear Materials, Volume 4*. Oxford, U.K.: Elsevier,

2012.

[33] S. J. Zinkle, H. Tanigawa, and B. D. Wirth, “Radiation and Thermomechanical Degradation Effects in Reactor Structural Alloys,” in *Structural Alloys for Nuclear Engineering Applications*, Cambridge: Elsevier, 2019, pp. 163–210.

[34] R. G. Odette and S. J. Zinkle, *Structural Alloys for Nuclear Energy Applications*. Elsevier, 2020.

[35] S. J. Zinkle, *Radiation-induced effects on microstructure*, vol. 1. Elsevier Inc., 2012.

[36] R. K. Nanstad, D. A. McClintock, D. T. Hoelzer, L. Tan, and T. R. Allen, “High temperature irradiation effects in selected Generation IV structural alloys,” *J. Nucl. Mater.*, vol. 392, no. 2, pp. 331–340, 2009.

[37] J. E. Pawel, A. F. Rowcliffe, G. E. Lucas, and S. J. Zinkle, “Irradiation performance of stainless steels for ITER application,” *J. Nucl. Mater.*, vol. 239, no. 1–3, pp. 126–131, 1996.

[38] F. A. Garner, M. L. Hamilton, N. F. Panayotou, and G. D. Johnson, “The microstructural origins of yield strength changes in AISI 316 during fission or fusion irradiation,” *J. Nucl. Mater.*, vol. 103–104, pp. 803–807, 1981.

[39] M. Victoria *et al.*, “Microstructure and associated tensile properties of irradiated fcc and bcc metals,” *J. Nucl. Mater.*, vol. 276, no. 1, pp. 114–122, 2000.

[40] E. R. Gilbert and J. F. Bates, “Dependence of irradiation creep on temperature and atom displacements in 20% cold worked type 316 stainless steel,” *J. Nucl. Mater.*, vol. 65, no. C, pp. 204–209, 1977.

[41] F. A. Garner, *Radiation damage in austenitic steels*, vol. 4. Elsevier Inc., 2012.

[42] S. Nogami, K. Abe, A. Hasegawa, K. Imasaki, and T. Tanno, “High-Temperature Helium Embrittlement of 316FR Steel,” *J. Nucl. Sci. Technol.*, vol. 48, no. 1, pp. 130–134, 2012.

[43] V. Fidleris, “The irradiation creep and growth phenomena,” *J. Nucl. Mater.*, vol. 159, no. C, pp. 22–42, 1988.

[44] F. A. Garner and D. S. Gelles, “Neutron-Induced Swelling of Commercial Alloys at Very High Exposures,” *Effects of Radiation on Materials: 14th International Sym- posium {Volume II)*. pp. 673–683, 1990.

[45] R. M. Boothby, *Radiation effects in nickel-based alloys*, vol. 4. Elsevier Inc., 2012.

[46] S. J. Zinkle and G. S. Was, “Materials challenges in nuclear energy,” *Acta Mater.*, vol. 61, no. 3, pp. 735–758, 2013.

[47] B. Raj and M. Vijayalakshmi, *Ferritic steels and advanced ferritic-martensitic steels*, vol. 4. Elsevier Inc., 2012.

[48] F. A. Garner, “Recent insights on the swelling and creep of irradiated austenitic alloys,” *J. Nucl. Mater.*, vol. 122, no. 1–3, pp. 459–471, 1984.

[49] F. A. Garner and H. R. Brager, “Dependence of neutron-induced swelling on composition in iron-based austenitic alloys,” 1984.

[50] H. Schroeder, “High Temperature Embrittlement of Metals By Helium.,” *Radiat. Eff.*, vol. 78, no. 1–4, pp. 297–314, 1983.

[51] P. Spatig, J. Chen, and G. R. Odette, “Ferritic and Tempered Martensitic Steels,” in *Structural Alloys for Nuclear Engineering Applications*, Cambridge: Elsevier, 2019, pp. 485–527.

[52] H. Schroeder and U. Stamm, “High Temperature Helium Embrittlement: Austenitic Versus Martensitic Stainless Steels,” *Eff. Radiat. Mater. 14th Int. Symp. (Volume I)*, pp. 223-223–23, 2009.

[53] M. L. Grossbeck, K. Ehrlich, and C. Wassilew, “An assessment of tensile, irradiation creep, creep rupture, and fatigue behavior in austenitic stainless steels with emphasis on spectral effects,” *J. Nucl. Mater.*, vol. 174, no. 2–3, pp. 264–281, 1990.

[54] C. Wassilew, W. Schneider, and K. Ehrlich, “Creep and creep-rupture properties of type 1.4970 stainless steel during and after irradiation,” *Radiat. Eff.*, vol. 101, no. 1–4, pp. 201–219, 1987.

[55] K. Anderko, L. Schaefer, C. Wassilew, L. Ehrlich, and H. J. Bergmann, “Mechanical properties of irradiated austenitic stainless steel 1.4970,” in *Radiation Effects in Breeder Reactor Structural Materials*, 1977.

[56] H. Ullmaier, “Helium in fusion materials: High temperature embrittlement,” *J. Nucl. Mater.*, vol. 133–134, no. C, pp. 100–104, 1985.

[57] S. Ukai, S. Mizuta, T. Kaito, and H. Okada, “In-reactor creep rupture properties of 20% CW modified 316 stainless steel,” *J. Nucl. Mater.*, vol. 278, no. 2, pp. 320–327, 2000.

[58] J. R. Lindgren, “Irradiation Effects on High-Temperature Gas-Cooled Reactor Structural Materials,” *Nucl. Technol.*, vol. 66, no. 3, pp. 607–618, 2017.

[59] K. Watanabe, T. Kondo, and Y. Ogawa, “Postirradiation Tensile and Creep Properties of Heat-Resistant Alloys,” *Nucl. Technol.*, vol. 66, no. 3, pp. 630–638, 2017.

[60] F. Garzarolli, K. P. Francke, and J. Fischer, “Influence of Neutron Irradiation on Tensile and Stress Rupture Properties of Inconel 625,” *J. Nucl. Mater.*, vol. 30, pp. 242–246, 1969.

[61] S. Xu, W. Zheng, and L. Yang, “A review of irradiation effects on mechanical properties of candidate SCWR fuel cladding alloys for design considerations,” *CNL Nucl. Rev.*, vol. 5, no. 2, pp. 309–331, 2016.

[62] D. F. Kharitonov, “Effect of Neutron Irradiation on Low-Cycle Fatigue of Structural Materials (Review),” *Strength Mater.*, vol. 16, no. 11, pp. 1594–1602, 1984.

[63] N. V. Luzginova, J. W. Rensman, M. Jong, P. Ten Pierick, T. Bakker, and H. Nolles, “Overview of 10 years of irradiation projects on Eurofer97 steel at High Flux Reactor in Petten,” *J. Nucl. Mater.*, vol. 455, no. 1–3, pp. 21–25, 2014.

[64] P. Marmy and B. M. Oliver, “High strain fatigue properties of F82H ferritic-martensitic steel under proton irradiation,” *J. Nucl. Mater.*, vol. 318, pp. 132–142, 2003.

[65] R. Lindau and A. Moslang, “Fatigue Tests on a Ferritic-Martensitic Steel At 420-Degrees-

C - Comparison Between in-Situ and Postirradiation Properties," *J. Nucl. Mater.*, vol. 212, no. A, pp. 599–603, 1994.

[66] R. Scholz and R. Mueller, "The effect of hold-times on the fatigue behavior of type AISI 316L stainless steel under deuteron irradiation," *J. Nucl. Mater.*, vol. 258–263, pp. 1600–1605, 1998.

[67] R. Scholz and R. Mueller, "The effect of hold-times on the fatigue life of 20% cold-worked Type 316L stainless steel under deutron irradiation," *J. Nucl. Mater.*, vol. 224, pp. 311–313, 1995.

[68] C. R. Brinkman, G. E. Korth, and R. R. Hobbins, "Estimates of Creep-Fatigue Interaction in Irradiated and Unirradiated Austenitic Stainless Steels," *Nucl. Technol.*, vol. 16, no. 1, pp. 297–307, 1972.

[69] C. R. Brinkman, J. M. Beeston, and G. E. Korth, "Fatigue and Creep-fatigue Behavior of Irradiated Stainless Steels -- Available Data, Simple Correlations, and Reccomendations for Additional Work in Support of LMFBR Design," 1973.

[70] G. S. Was and T. R. Allen, "Corrosion Issues in Current and Next-Generation Nuclear Reactors," in *Structural Alloys for Nuclear Engineering Applications*, Cambridge: Elsevier, 2019, pp. 211–246.

[71] K. Tuček, J. Carlsson, and H. Wider, "Comparison of sodium and lead-cooled fast reactors regarding reactor physics aspects, severe safety and economical issues," *Nucl. Eng. Des.*, vol. 236, no. 14–16, pp. 1589–1598, 2006.

[72] K. Natesan, M. Li, O. K. Chopra, and S. Majumdar, "Sodium effects on mechanical performance and consideration in high temperature structural design for advanced reactors," *J. Nucl. Mater.*, vol. 392, no. 2, pp. 243–248, 2009.

[73] R. Kannan *et al.*, "Influence of dynamic sodium environment on the creep-fatigue behaviour of Modified 9Cr-1Mo ferritic-martensitic steel," *Nucl. Eng. Des.*, vol. 241, no. 8, pp. 2807–2812, 2011.

[74] D. Gorse *et al.*, "Influence of liquid lead and lead-bismuth eutectic on tensile, fatigue and creep properties of ferritic/martensitic and austenitic steels for transmutation systems," *J. Nucl. Mater.*, vol. 415, no. 3, pp. 284–292, 2011.

[75] S. A. Maloy, K. Natesan, D. E. Holcomb, C. Fazio, and P. Yvon, "Overview of Reactor Systems and Operational Environments for Structural Materials in Gen-IV Fission Reactors," in *Structural Alloys for Nuclear Engineering Applications*, Cambridge: Elsevier, 2019, pp. 23–49.

[76] T. L. Lin, Y. H. Zhang, and H. W. Yang, "Influence of hot corrosion on the creep strength of the nickel-base superalloy GH37," *Mater. Sci. Eng.*, vol. 62, no. 1, pp. 17–24, 1984.

[77] M. Yoshiba, O. Miyagawa, H. Mizuno, and H. Fujishiro, "Effect of Environmental Factors on the Creep Rupture Properties of a Nickel-Base Superalloy Subjected to Hot Corrosion," *Trans. Japan Inst. Met.*, vol. 29, no. 1, pp. 26–41, 1988.

[78] V. Suryanarayanan, K. J. L. Iyer, and V. M. Radhakrishnan, "Interaction of low temperature

hot corrosion and creep," *Mater. Sci. Eng. A*, vol. 112, no. C, pp. 107–116, 1989.

[79] S. Ahila and S. R. Iyer, "Creep rupture behaviour of 2.25Cr-1Mo steel in sulphate-pyrosulphate mixture," *J. Mater. Sci. Lett.*, vol. 12, no. 24, pp. 1925–1926, 1993.

[80] J. G. González-Rodríguez, A. Luna-Ramírez, and A. Martínez-Villafañe, "Effect of hot corrosion on the creep properties of types 321 and 347 stainless steels," *J. Mater. Eng. Perform.*, vol. 8, no. 1, pp. 91–97, 1999.

[81] A. Homaeian and M. Alizadeh, "Interaction of hot corrosion and creep in Alloy 617," *Eng. Fail. Anal.*, vol. 66, pp. 373–384, 2016.

[82] V. Mannava, A. Sambasivarao, N. Paulose, M. Kamaraj, and R. S. Kottada, "An investigation of oxidation/hot corrosion-creep interaction at 800 °C in a Ni-base superalloy coated with salt mixture deposits of Na2SO4-NaCl-NaVO3," *Corros. Sci.*, vol. 147, no. November 2018, pp. 283–298, 2019.

[83] P. S. Shankar and K. Natesan, "Effect of trace impurities in helium on the creep behavior of Alloy 617 for very high temperature reactor applications," *J. Nucl. Mater.*, vol. 366, no. 1–2, pp. 28–36, 2007.

[84] K. Natesan and P. S. Shankar, "Uniaxial creep response of Alloy 800H in impure helium and in low oxygen potential environments for nuclear reactor applications," *J. Nucl. Mater.*, vol. 394, no. 1, pp. 46–51, 2009.

[85] F. Rouillard, C. Cabet, K. Wolski, and M. Pijolat, "Oxide-layer formation and stability on a nickel-base alloy in impure helium at high temperature," *Oxid. Met.*, vol. 68, no. 3–4, pp. 133–148, 2007.

[86] M. Cappelaere, M. Perrot, and J. Sannier, "Behavior of Metallic Materials Between 550 and 870 degree C in High-Temperature Gas-Cooled Reactor Helium Under Pressures of 2 and 50 Bar," *Nucl. Technol.*, vol. 66, no. 2, pp. 465–478, 1984.

[87] L. W. Graham, "Corrosion of metallic materials in HTR-helium environments," *J. Nucl. Mater.*, vol. 171, no. 1, pp. 76–83, 1990.

[88] W. J. Quadakkers, "High temperature corrosion in the service environments of a nuclear process heat plant," *Mater. Sci. Eng.*, vol. 87, no. C, pp. 107–112, 1987.

[89] Y. Hosoi and S. Abe, "The effect of helium environment on the creep rupture properties of Inconel 617 at 1000°C," *Metall. Trans. A*, vol. 6, no. 6, pp. 1171–1178, 1975.

[90] B. Huchtemann, "The effect of alloy chemistry on creep behaviour in a helium environment with low oxygen partial pressure," *Mater. Sci. Eng. A*, vol. 120–121, no. PART 2, pp. 623–626, 1989.

[91] L. R. Liu *et al.*, "Effect of carbon addition on the creep properties in a Ni-based single crystal superalloy," *Mater. Sci. Eng. A*, vol. 385, no. 1–2, pp. 105–112, 2004.

[92] R. H. Cook, "Creep Properties of Inconel-617 in Air and Helium at 800 to 1000 degree C," *Nucl. Technol.*, vol. 66, no. 2, pp. 283–288, 1984.

[93] H. Tsuji and T. Kondo, "Low-Cycle Fatigue of Heat-Resistant Alloys in High-Temperature

Gas-Cooled Reactor Helium.," *Nucl. Technol.*, vol. 66, no. 2, pp. 347–353, 1984.

[94] K. Bhanu Sankara Rao, H. P. Meurer, and H. Schuster, "Creep-fatigue interaction of inconel 617 at 950°C in simulated nuclear reactor helium," *Mater. Sci. Eng.*, vol. 104, no. C, pp. 37–51, 1988.

[95] M. C. Messner, R. I. Jetter, Y. Wang, and T.-L. Sham, "Initial Development of an Improved Creep-Fatigue Design Method that Avoids the Separate Evaluation of Creep and Fatigue Damage and Eliminates the Requirement for Stress Classification," 2019.

[96] M. C. Messner, V.-T. Phan, R. I. Jetter, and T.-L. Sham, "The Mechanical Interaction of Clad and Base Metal for Molten Salt Reactor Structural Components," in *Proceedings of the 2018 ASME Pressure Vessels and Piping Conference*, 2018, pp. PVP2018-84101.

[97] B. Barua, B. Jetter, V.-T. Phan, T.-L. Sham, M. C. Messner, and Y. Wang, "Design methodologies for high temperature reactor structural components cladded with noncompliant materials," in *Proceedings of the 2019 ASME Pressure Vessels and Piping Conference*, 2019, pp. PVP2019-93643.

[98] B. Barua, M. C. Messner, B. Jetter, and T.-L. Sham, "Development of Design Method for High Temperature Nuclear Reactor Cladded Components," in *Proceedings of the 2020 ASME Pressure Vessels and Piping Conference*, 2020, pp. PVP2020-21469.

[99] B. Barua, M. C. Messner, R. I. Jetter, and T.-L. Sham, "Selection Criteria for Clad Materials to use with a 316H Base Material for High Temperature Nuclear Reactor Cladded Components," in *Proceedings of the 2020 ASME Pressure Vessels and Piping Conference*, 2020, pp. PVP2020-21493.

[100] B. Barua, M. C. Messner, A. Rovinell, and T.-L. Sham, "Acceptance Criteria for the Mechanical Integrity of Clad/Base Metal Interface for High Temperature Nuclear Reactor Cladded Components," in *Proceedings of the 2020 ASME Pressure Vessels and Piping Conference*, 2020, pp. PVP2020-21494.

[101] M. C. Messner, V.-T. Phan, R. I. Jetter, and T.-L. Sham, "Assessment of Passively Actuated In-Situ Cyclic Surveillance Test Specimens for Advanced Non-Light Water Reactors," in *Proceedings of the ASME 2018 Pressure Vessels and Piping Conference*, 2018, pp. PVP2018-84793.

Applied Materials Division
Argonne National Laboratory
9700 South Cass Avenue, Bldg. 212
Argonne, IL 60439

www.anl.gov